EJECTION OF THE MASSIVE HYDROGEN-RICH ENVELOPE TIMED WITH THE COLLAPSE OF THE STRIPPED
SN 2014C

Raffaella Margutti[1,2], A. Kamble[2], D. Milisavljevic[2], S. de Mink[3], E. Zapartas[3], M. Drout[2], R. Chornock[4], G. Risaliti[5], B. A. Zauderer[2], M. Bietenholz[6,7], M. Cantiello[8], S. Chakraborti[2], L. Chomiuk[9], W. Fong[10], B. Grefenstette[11], C. Guidorzi[12], R. Kirshner[2], J. T. Parrent[2], D. Patnaude[2], A. M. Soderberg[2], N. C. Gehrels[13], F. Harrison[14]

Draft version January 27, 2016

ABSTRACT

We present multi-wavelength observations of Supernova 2014C during the first 500 days of its evolution. These observations represent the first solid detection of a young extragalactic stripped-envelope SN out to high-energy X-rays ~ 40 keV. SN 2014C was the explosion of an envelope-stripped progenitor star with ordinary explosion parameters ($E_k \sim 1.8 \times 10^{51}$ erg and $M_{ej} \sim 1.7 \, M_\odot$). However, over the time scale of ~ 1 yr, SN 2014C experienced a complete metamorphosis and evolved from an ordinary hydrogen-poor supernova of type Ib into a strongly interacting, hydrogen-rich supernova of type IIn, thus violating the traditional classification scheme of type-I vs. type-II SNe. Signatures of the SN shock interacting with a dense medium are observed across the electromagnetic spectrum, from the radio to the hard X-ray band. Coordinated observations with Swift, Chandra and NuSTAR have captured the evolution in detail and revealed the presence of a massive shell of $\sim 1 \, M_\odot$ of hydrogen-rich material at $\sim 6 \times 10^{16}$ cm from the explosion site. We estimate that the shell was ejected by the progenitor star in the decades to centuries before core collapse. This result poses significant challenges to current theories of massive star evolution, as it requires a physical mechanism responsible for the ejection of the deepest hydrogen layer of H-poor SN progenitors synchronized with the onset of stellar collapse. Theoretical investigations point at binary interactions and/or instabilities during the last stages of nuclear burning in massive stars as potential triggers of the highly time-dependent mass loss. We constrain these scenarios utilizing the sample of 183 SNe Ib/c with public radio observations. Our analysis identifies SN 2014C-like signatures, consistent with strong interaction, in $\sim 10\%$ of SNe with constraining radio data. This fraction is somewhat larger but reasonably consistent with the expectation from the theory of recent envelope ejection due to binary evolution *if* the ejected material can survive in the close environment for $10^3 - 10^4$ yrs. Alternatively, nuclear burning instabilities extending all the way to the core C-burning phase might also play a critical role.

Subject headings: supernovae: specific (SN 2014C)

1. INTRODUCTION

[1] Center for Cosmology and Particle Physics, New York University, 4 Washington Place, New York, NY 10003, USA

[2] Harvard-Smithsonian Center for Astrophysics, 60 Garden St., Cambridge, MA 02138, USA

[3] Anton Pannenkoek Institute for Astronomy, University of Amsterdam, 1090 GE Amsterdam, The Netherlands

[4] Astrophysical Institute, Department of Physics and Astronomy, 251B Clippinger Lab, Ohio University, Athens, OH 45701, USA

[5] INAF-Arcetri Astrophysical Observatory, Largo E. Fermi 5, I-50125 Firenze, Italy

[6] Department of Physics and Astronomy, York University, Toronto, ON M3J 1P3, Canada

[7] Hartebeesthoek Radio Observatory, PO Box 443, Krugersdorp 1740, South Africa

[8] Kavli Institute for Theoretical Physics, University of California, Santa Barbara, CA 93106, USA

[9] Department of Physics and Astronomy, Michigan State University, East Lansing, MI 48824, USA

[10] Steward Observatory, University of Arizona, 933 North Cherry Avenue, Tucson, AZ 85721, USA

[11] Cahill Center for Astrophysics, 1216 E. California Blvd., California Institute of Technology, Pasadena, CA 91125, USA

[12] University of Ferrara, Department of Physics and Earth Sciences, via Saragat 1, ID44122 Ferrara, Italy

[13] NASA Goddard Space Flight Center, Code 661, Greenbelt, MD 20771, USA

[14] Space Radiation Laboratory, California Institute of Technology, 1200 E California Blvd, MC 249-17, Pasadena, CA 91125, USA

Mass loss from massive stars ($> 10 \, M_\odot$) plays a major role in the chemical enrichment of the Universe and directly determines the luminosity, lifetime and fate of stars. Yet, the dominant channels and the physical mechanisms that drive mass loss in evolved massive stars are uncertain (see Smith 2014 for a recent review). This lack of understanding is significant as it further impacts our estimates of the stellar initial mass function in galaxies and star formation through cosmic time, which rely on the predictions of stellar evolution models (Bastian et al. 2010, Madau et al. 1998, Hopkins & Beacom 2006).

Relevant observations that expose our inadequate theoretical understanding of mass loss in evolved massive stars include the discovery of powerful eruptions prior to major explosions in H-rich massive stars, of which SN 2009ip is the best studied example (e.g. Mauerhan et al. 2013, Pastorello et al. 2013, Margutti et al. 2014a, Smith 2014 and references therein; Ofek et al. 2013, Ofek et al. 2014; Fraser et al. 2013). A precursor to the SN explosion has also been identified in the case of the type-Ibn SN 2006jc, which showed signs of interaction with a He-rich medium (e.g. Foley et al. 2007, Pastorello et al. 2007). Evidence for significantly enhanced mass loss timed with the explosion has been found for the H-poor progenitors of both type-IIb SNe (Kamble et al. 2015, Maeda et al. 2015) and type-Ib SNe (Svirski & Nakar 2014), as well as for the H- and He-poor progenitors of type-Ic SNe asso-

ciated with some nearby gamma-ray bursts (Margutti et al. 2015, Nakar 2015). Along the same line, it is relevant to mention the possible detection of an outburst from the progenitor of the type-Ic SN PTF11qcj ~ 2.5 yrs before stellar death (Corsi et al. 2014), the evidence for significant temporal variability in the radio light-curves of Ib/c SNe (Soderberg 2007, Wellons et al. 2012) and the recent detection of interaction of the H-poor super-luminous SN iPTF13ehe with H-rich material at late-times (Yan et al. 2015).

These observations point to the presence of strongly time-dependent mass loss synchronized with core-collapse in a variety of stellar explosions (from type-IIn SNe to ordinary Ib/c, gamma-ray burst SNe and even super-luminous SNe). The erratic behavior of these stars approaching stellar death across the mass spectrum clearly deviates from the commonly accepted picture of steady mass loss through line-driven winds employed by current models of stellar evolution (e.g. Smith 2014). However, the nature of the physical process responsible for the highly time-dependent mass loss is at the moment a matter of debate. Equally unclear is the extent to which these processes have an active and important role in the evolutionary path that leads to the envelope-stripped progenitors of ordinary hydrogen-poor core-collapse SNe (i.e. SNe of type Ib/c). We address this still-open question in our study of SN 2014C in the context of 183 Ib/c radio SNe.

We present multi-wavelength observations of the remarkable metamorphosis of SN 2014C, which evolved from an ordinary H-stripped core-collapse SN of type Ib into a strongly interacting type-IIn SN over ~ 1 yr of observations. The relative proximity of SN 2014C in NGC 7331 (d=14.7 Mpc, Freedman et al. 2001) allowed us to witness the progressive emergence of observational signatures of the undergoing interaction across the electromagnetic spectrum, and, in particular, it offered us the unprecedented opportunity to follow the development of luminous X-ray emission captured in detail by the Swift X-ray Telescope (XRT), the Chandra X-ray Observatory (CXO) and the Nuclear Spectroscopic Telescope Array (NuSTAR). SN 2014C is the first young H-stripped SN for which we have been able to follow the evolution in the hard X-ray range. SN 2014C is also the first envelope-stripped SN that showed a mid-InfraRed re-brightening in the months after the explosion (Tinyanont et al. 2016).

This paper is organized as follows. UV, optical, X-ray and hard X-ray observations of SN 2014C are described in Sec. 2. The explosion properties of SN 2014C are derived in Sec. 3. We interpret the metamorphosis of SN 2014C in the context of strong SN shock interaction with dense and massive H-rich material that was ejected by the progenitor star during the years before core-collapse. We derive mass, density, distance and time of ejection of the H-rich shell in Sec. 4. We put SN 2014C into the context of Ib/c SNe and constrain the rate of 14C-like events among 183 Ib/c SNe observed at radio frequencies in Sec. 5. Based on these results, we discuss the challenges faced by the current theories of massive star evolution and explore alternatives in Sec. 6. We conclude in Sec. 7. Details of the spectroscopic evolution of SN 2014C are provided in Milisavljevic et al. (2015) (hereafter M15), while we refer to Kamble et al., 2015 (hereafter K15) for the modeling of the radio synchrotron emission which originates from the SN shock interaction with the medium.

Accurate modeling of the bolometric light-curve of SN 2014C of Sec. 3 constrains the time of first light to December 30, 2013 ± 1 day (MJD 56656 ± 1, see Sec. 3). Times will be referred to MJD 56656 unless explicitly noted.
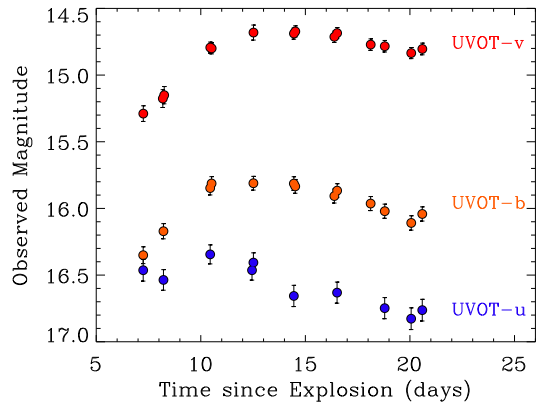

FIG. 1.— Temporal evolution of SN2014C in u, b and v band as captured by Swift-UVOT. No host subtraction and extinction correction have been applied.
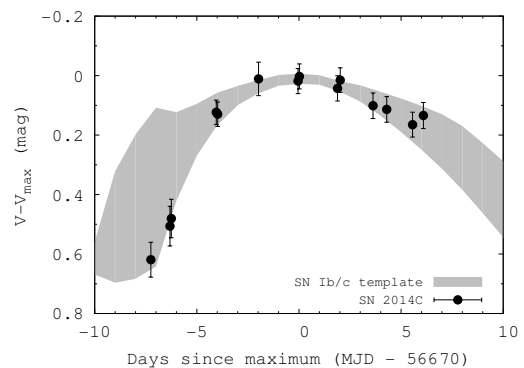

FIG. 2.— Temporal evolution of the v-band emission from SN 2014C as observed by *Swift*-UVOT, compared to the SNe Ibc template from Drout et al. (2011). The width of the grey curve is derived from the 1σ deviation from the mean at each epoch.

M15 estimate $E(B-V)_{tot} \sim 0.75$ mag in the direction of the transient, which we will use to correct our photometry. The Galaxy only contributes a limited fraction, corresponding to $E(B-V)_{mw} = 0.08$ mag (Schlafly & Finkbeiner 2011). Local extinction thus clearly dominates over the Galactic value, suggesting the presence of large quantities of material in NGC 7331 towards SN 2014C. Finally, uncertainties are quoted at the level of 1σ confidence level unless stated otherwise.

2. OBSERVATIONS AND DATA REDUCTION

2.1. *Optical-UV Photometry with Swift-UVOT*

The UV-Optical Telescope (UVOT, Roming et al. 2005) onboard the *Swift* satellite (Gehrels et al. 2004) started observing SN 2014C on January 6, 2014 (PIs P. Milne and R. Margutti). Due to its angular proximity to the Sun, SN 2014C was not observable by *Swift* in the time periods late January-April 2014 and February-March 2015. We employed the latest HEAsoft release (v. 6.16) with the corresponding calibration files to reduce the data and a source extraction region of 3" to minimize the contamination from host-galaxy light. We extracted the photometry following the prescriptions by Brown et al. (2009).

SN 2014C is clearly detected in the wave-length range 3500-5500 Å (i.e. UVOT u, b and v filters) between −7 days and +7 days since maximum light (MJD 56663 $<t<$ MJD 56677). In the same time period SN 2014C is only marginally detected in the UV (i.e. UVOT $w1$, $w2$ and $m2$ filters), mainly

because of bright and diffuse UV emission from the host galaxy at the location of the SN. SN 2014C reaches v-band maximum light around January 13, 2014 (MJD 56670). A search for increased UV emission arising from the SN shock interaction with the massive CSM in late-time ($t > 6$ months) UVOT data led to a non-detection. Table 3 reports the complete UVOT photometry.

A comparison of the v-band light-curve of SN 2014C to the SN Ibc template by Drout et al. (2011) in Figure 2 illustrates that its rise time to maximum light of ~ 14 days falls on the short end of the observed distribution. The overall shape of the light-curve is however in reasonable agreement with the template, which indicates a rather standard ejecta mass (M_{ej}) to kinetic energy (E_k) ratio, as quantified in Sec. 3.

2.2. Deep Late-time Optical Photometry with MMTCam

We obtained $r'i'$−band observations of SN 2014C with the MMTCam imager mounted on the 6.5m MMT on 5 epochs spanning May 18, 2014 to May 23, 2015 (139 to 509 days since explosion, PI Margutti). All frames were bias, dark, and flat field corrected using standard tasks in IRAF[15]. PSF photometry was performed on all images and absolute calibration was performed using five SDSS stars in a nearby standard field. The resulting photometry is listed in Table 4 and shown in Figure 10. No template subtraction was performed as the source was still visible in our final epoch of observation, and no sufficiently deep archival images were available in these bands. During our final epochs of observation the source is ~ 0.6 mag brighter than the R-band pre-explosion source described in M15.

2.3. Early-time X-ray observations with Swift-XRT

The *Swift* X-Ray Telescope (XRT, Burrows et al. 2005) started observing SN 2014C on ($\delta t \sim 7$ days since explosion, PI P. Milne). Observations acquired before SN 2014C set behind the Sun cover the time interval $t \sim 7-20$ days since the explosion, with a total exposure time of 17.2 ks. We detect significant X-ray emission at the SN site. However, inspection of pre-explosion images acquired in 2007 reveals the presence of diffuse X-ray emission that is not spatially resolved by the XRT. By accounting for the unresolved host-galaxy contribution, as constrained from pre-explosion observations, we infer a 3σ limit to the SN emission of $8.1 \times 10^{-4}\,\mathrm{c\,s^{-1}}$ (0.3-10 keV).

Coordinated observations of the Chandra X-ray Observatory and NuSTAR obtained at later times (Sec. 2.4 and 2.5) showed evidence for large intrinsic neutral hydrogen absorption in the direction of SN 2014C. At the time of the first Chandra observations we infer a total hydrogen column density $\mathrm{NH_{tot}} \lesssim 4 \times 10^{22}\,\mathrm{cm^{-2}}$ (Sec. 2.6). The Galactic hydrogen column density is $\mathrm{NH_{mw}} \lesssim 6.1 \times 10^{20}\,\mathrm{cm^{-2}}$ (Kalberla et al. 2005). The measured hydrogen column is thus dominated by material in the host galaxy of SN2014C. Restricting our analysis to the 2-10 keV energy range to minimize the impact of the uncertain absorption of soft X-rays, and accounting for the unresolved host-galaxy contribution, we infer a 3σ limit to the SN emission of $3.0 \times 10^{-4}\,\mathrm{c\,s^{-1}}$ (2-10 keV). For $\mathrm{NH_{tot}} \sim 5 \times 10^{22}\,\mathrm{cm^{-2}}$, the corresponding unaborbed flux limit is $F_x < 4.1 \times 10^{-14}\,\mathrm{erg\,s^{-1}cm^{-2}}$ and the luminosity limit is $L_x < 1.1 \times 10^{39}\,\mathrm{erg\,s^{-1}}$ (2-10 keV). We assume a power-law
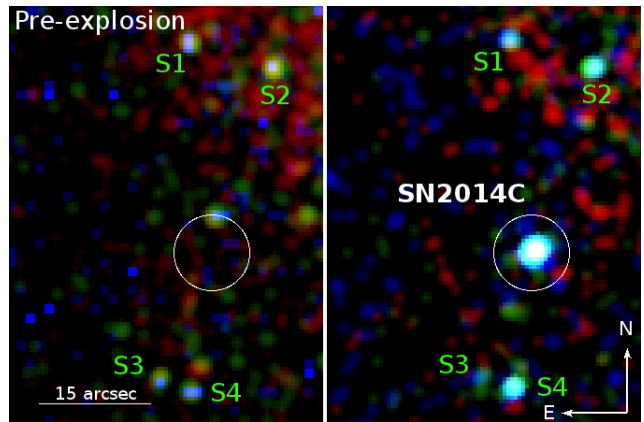
FIG. 3.— Pre- and post-explosion, false-color composite X-ray images at the location of SN 2014C taken with Chandra. In both panels we use red are for for the 0.3-1 keV energy band, green for 1-3 keV photons while blue-to-white shades mark the hardest photons in the images with energy 3-10 keV. The pre-explosion image collects 29.5 ks of observations acquired in 2001. The right panel collects the post-explosion Chandra data presented in this paper (exposure time of 29.7 ks), covering the time period November 2011-April 2015. SN 2014C is well detected in this time period as a bright source of hard X-ray emission. White circle: 5" radius region at the position of SN 2014C.

spectral model with photon index $\Gamma = 2$, as appropriate for non-thermal Inverse Compton (IC) emission (see Sec. 4).

2.4. Deep X-ray observations with Chandra

Pre-Explosion: The field of SN 2014C was observed by the Chandra X-ray Observatory (CXO) on January 27th, 2001 (PI Zezas, ID 2198). In 29.5 ks of observations we find no evidence for X-ray emission at the SN site down to the limit of $2.6 \times 10^{-4}\,\mathrm{c\,s^{-1}}$ (0.3-10 keV). For an assumed power-law spectrum with photon index $\Gamma = 2$ the value above converts into an absorbed flux $< 2.8 \times 10^{-15}\,\mathrm{erg\,s^{-1}\,cm^{-2}}$ (0.3-10 keV), which corresponds to $L_x < 8.5 \times 10^{37}\,\mathrm{erg\,s^{-1}}$ (0.3-10 keV).

Post-Explosion: We started a monitoring campaign with the CXO to constrain the evolution of SN 2014C under our approved program to monitor SNe originating from hydrogen stripped progenitors in the local Universe. A first observation was obtained on November 3, 2014 ($t = 308$ days, PI A. Soderberg, ID 16005), followed by a number of observations during 2015 under a multi-epoch DDT program (PI R. Margutti, IDs 17569, 17570, 17571).

CXO data have been reduced with the CIAO software package (version 4.6) and corresponding calibration files. Standard ACIS data filtering has been applied. SN 2014C is a bright source of X-ray emission with luminosity increasing with time (Fig. 3 and Fig. 6). In our first epoch at $t = 308$ days, SN 2014C is detected at the level of $> 40\sigma$, with a net count-rate of $0.013\,\mathrm{c\,s^{-1}}$ (0.5-8 keV, exposure time of 9.9 ks). A spectral fit with an absorbed power-law model $F_\nu \propto \nu^{-\beta}$ indicates very hard emission with index $\beta = -1.5 \pm 0.3$. The detected X-ray emission is also in significant excess with respect to the extrapolation of the synchrotron spectrum that best fits the radio observations at all times (Fig. 5). These two findings together suggest a thermal origin for the X-rays (as confirmed by coordinated CXO-NuSTAR observations obtained later). A fit with an absorbed bremsstrahlung model constrains $T > 10$ keV. We estimate the absorption at $t = 308$ days as follows. Chandra and NuSTAR observations obtained ~ 90 days later, at $t = 396$ days, are well modeled by a thermal bremsstrahlung spectrum with $T \sim 18$ keV (Sec. 2.6). The interaction of the SN shock with a very dense medium
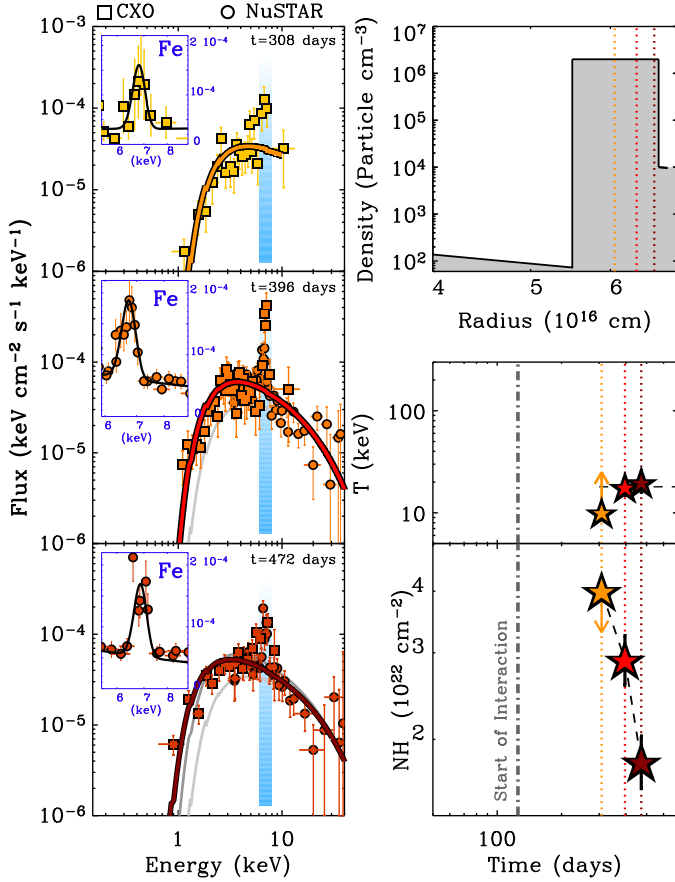
FIG. 4.— Coordinated CXO (squares) and NuSTAR (filled dots) observations of SN 2014C revealed an X-ray thermally emitting plasma with characteristic temperature $T \sim 20$ keV and an absorption decreasing with time (middle and bottom panels on the right). The best fitting bremsstrahlung model is represented with a thick colored line in each panel on the left and reproduced with grey lines in the other panels for comparison. An excess of emission around 6.7-6.9 keV is clearly detected at all epochs. We associate this emission with He-like and H-like Fe transitions. The upper right panel potrays the density profile of the environment as constrained by these observations and our modeling in Sec. 4.
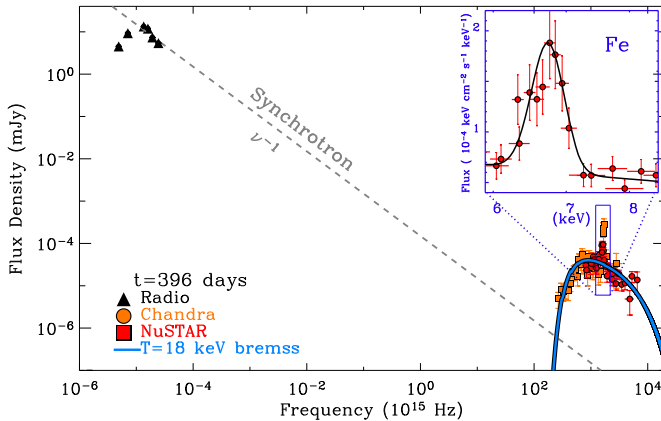

FIG. 5.— Radio (VLA from K15) to hard X-ray (CXO, NuSTAR) spectral energy distribution of SN 2014C at $t = 396$ days after the explosion, shown here as an example. The X-ray emission is in clear excess to the synchrotron model that best fits the radio observations, as expected in the case of SN shock interaction with a very dense medium (e.g. Chevalier & Fransson 2006). CXO and NuSTAR data are best fit by an absorbed bremsstrahlung model with $T \sim 18$ keV and $NH_{tot} \sim 3 \times 10^{22}$ cm^{-2}. Emission at 6.7-6.9 keV due to H-like and He-like Fe transitions is also clearly detected (*Inset*).
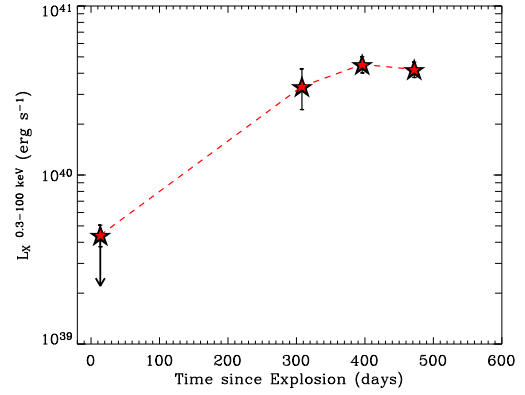

FIG. 6.— Broad-band X-ray light-curve of SN 2014C during the first 500 days as captured by Swift, the CXO and NuSTAR.

causes a rapid deceleration of the forward shock accompanied by a sudden and marked increase of the reverse shock temperature. At later times the temperatures of the forward and reverse shock decrease (see e.g. Chugai & Chevalier 2006, their Fig 2). SN 2014C started to interact with the dense shell ~ 100 days after the explosion (M15, i.e. ~ 200 days before the coordinated CXO-NuSTAR follow up, Sec. 4), which implies $T > 18$ keV at $t = 308$ days. Using this constraint to the temperature in our absorbed bremsstrahlung fit to the CXO data, we infer $NH_{tot} \lesssim 4 \times 10^{22}$ cm^{-2} at $t = 308$ days.

Ninety days later, ($t = 396$ days), our campaign reveals that SN 2014C substantially brightened with time, reaching $0.026 \, \mathrm{c \, s^{-1}}$ in the 0.5-8 keV band ($> 90\sigma$ significance level detection using 9.9 ks of observations). From the spectral analysis it is clear that the re-brightening is more apparent at soft X-ray energies ($E \lesssim 4$ keV), pointing to a decreased neutral hydrogen column density NH_{tot}. Our latest CXO observation was obtained at $t = 472$ days since explosion, with total exposure of 9.9 ks. SN 2014C is detected at the level of $0.0285 \, \mathrm{c \, s^{-1}}$ ($> 100\sigma$ significance level, 0.5-8 keV). The spectral parameters at $t = 396$ days and $t = 472$ days are best constrained by the joint CXO-NuSTAR fit described in Sec. 2.6. The results from our broad band X-ray spectral fits and the resulting luminosities are reported in Table 1. Finally, in each of the three CXO observations we note the presence of enhanced emission around 6.7-6.9 keV that we associate with H-like and He-like Fe line emission (Fig. 4).

2.5. *Hard X-ray observations with NuSTAR*

We obtained two epochs of observations with the Nuclear Spectroscopic Telescope Array (NuSTAR) under approved DDT and Guest Investigator programs (PI Margutti), coordinated in time with the CXO at $t = 396$ days and $t = 472$ days since explosion. Our programs led to the first detection of a young hydrogen-stripped core-collapse SN at hard X-rays energies. SN 2014C is well detected by NuSTAR in the energy range $3-40$ keV. The NuSTAR level 1 data products have been processed with the NuSTAR Data Analysis Software package version 1.4.1 included in the 6.16 HEASoft release. Event files were produced, calibrated, and cleaned using the standard filtering criteria and the latest files available in the NuSTAR calibration database (CALDB version 20150622). The total net exposures, after the exclusion of periods of source occultation by Earth and passages on the South Atlantic Anomaly, are 32.5 and 22.4 ks for the first and second observation, respectively. The source extraction radius is 1′ for both observations, and has been chosen in order to

TABLE 1
BROAD-BAND X-RAY SPECTRAL MODELING WITH THERMAL
BREMSSTRAHLUNG

Date (days)	Instrument	Temperature T (keV)	Absorption NH_{tot} (10^{22} cm^{-2})
308	CXO	> 10	$\lesssim 4$
396	CXO+NuSTAR	$17.8^{+3.7}_{-2.8}$	$2.9^{+0.4}_{-0.3}$
472	CXO+NuSTAR	$19.8^{+6.3}_{-3.9}$	$1.8^{+0.2}_{-0.2}$

TABLE 2
PROPERTIES OF THE FE LINE EMISSION MODELED WITH A GAUSSIAN
PROFILE

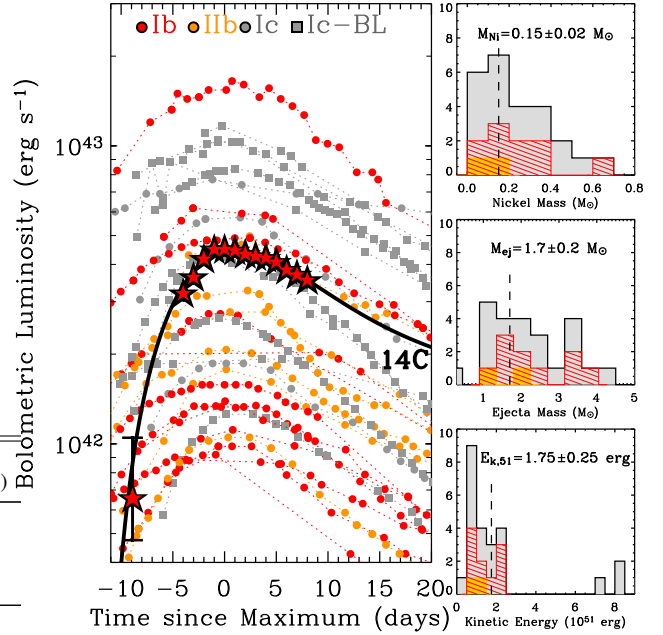| Date (days)	Instrument	Central Energy E (keV)	FWHM (keV)	Flux (10^{-13} erg s^{-1} cm^{-2})
308	CXO	6.80 ± 0.20	0.55 ± 0.23	(1.30 ± 0.30)
396	CXO+NuSTAR	6.70 ± 0.04	0.56 ± 0.09	(1.20 ± 0.10)
472	CXO+NuSTAR	6.84 ± 0.05	0.59 ± 0.14	(1.20 ± 0.10)

FIG. 7.— *Left Panel:* Bolometric luminosity and best-fitting model (thick black line) of SN 2014C in the context of well-monitored core-collapse SNe originating from stellar progenitors that had lost most of their hydrogen envelope before exploding (i.e. type Ic, Ic-BL, Ib and IIb). Data for the other SNe are from Cano (2013), Cano & Jakobsson (2014), Cano et al. (2014) and Lyman et al. (2014). *Right Panels:* Explosion parameters of SN 2014C (vertical dashed lines) compared to the sample of Drout et al. (2011). SN 2014C shows normal explosion parameters.

maximize the S/N ratio. The background has been extracted in source-free regions in the the field of view of each observation. The NuSTAR data are calibrated up to 79 keV, however a comparison between the source and the background counts show that the spectrum is background-dominated above 30-40 keV. Therefore we limited our spectral analysis to the range 3-40 keV. The higher energy bandpass of NuSTAR and the joint observations with the CXO at lower energies are crucial to constrain the temperature of the emitting region, the absorption column density of material in front of the emitting region and their evolution with time (Sec. 2.6).

2.6. *CXO-NuSTAR spectral modeling*

The CXO covers the energy range $0.3 - 10$ keV, while NuSTAR is sensitive between 3 and 79 keV. The two instruments have very different Point Spread Functions (PSF): while the CXO is able to spatially resolve the emission from SN 2014C from other sources in NGC7331 (Fig. 3), the composite emission appears as a single source at higher energies due to the wider instrumental PSF of NuSTAR (FWHM of 18"). The emission from other sources within the NuSTAR 1′ region is significantly fainter than SN 2014C. Nevertheless, to estimate and remove the contamination from other sources to the NuSTAR PSF we employed the CXO observations as follows. For both epochs we extracted a CXO spectrum of the contaminating sources by using an annular region with inner radius 1.5″ and outer radius of 1′ centered at the SN position. We model this spectrum with an absorbed power-law model to determine the best fitting spectral parameters of the contaminating emission, and extrapolate its contribution to the NuSTAR energy band. We then add a spectral component with these parameters to the model used for the spectral fitting of the NuSTAR data, only. As a refinement of the method above, we extracted a spectrum of each point-like source that we detected with the CXO within the NuSTAR extraction region and fit the spectrum of each source with an absorbed power-law function that we extrapolate to the NuSTAR energy band, obtaining consistent results.

Accounting for the contaminating emission to the NuSTAR data as described above, we find that the two epochs of co-ordinated CXO-NuSTAR observations are well fit by an absorbed thermal bremsstrahlung spectral model with tempera-

ture $T \sim 20$ keV and decreasing absorption with time (Fig. 4). We measure $NH_{tot} \sim 3 \times 10^{22}$ cm^{-2} and $NH_{tot} \sim 2 \times 10^{22}$ cm^{-2} at $t = 396$ days and $t = 472$ days, respectively. Table 1 reports the detailed results from the broad-band X-ray spectral fitting while the resulting X-ray light-curve of SN 2014C is portrayed in Fig. 6.

Finally, we find evidence an excess of emission around $\sim 6.7 - 6.9$ keV that we identify with H- and He-like transitions in Fe atoms. The Fe emission, as revealed by both the CXO and NuSTAR, is present in each of the three epochs of observations (Fig. 4 and 5) with no detectable evolution from one epoch to the other. The results from a spectral line fitting with a Gaussian profile are reported in Table 2. Our observations do not have the spectral resolution and statistics to resolve what is likely to be a complex of emission lines originating from highly ionized Fe atom states, as suggested by the calculations by Mewe et al. (1985), Mewe et al. (1986) and Liedahl et al. (1995) (e.g. the MEKAL model within Xspec).

3. EXPLOSION PARAMETERS

We calculate the bolometric luminosity of SN 2014C by integrating the extinction-corrected flux densities in the v, b and u UVOT bands and by applying a bolometric correction which corresponds to effective black-body temperatures in the range $7000 - 10000$ K. We complement this data set with public photometry, which allow us to constrain the very early light-curve. Specifically, SN 2014C was first detected on 2.10 UT January, 2014. Kim et al. (2014) reports a detection of SN 2014C at the level of $R = 17.1$ mag. Assuming a bolometric correction appropriate for a temperature of emission $T \sim 10000 - 15000$ K, we derive $L_{bol} = (0.5 - 10) \times 10^{41}$ erg s^{-1} at $t \sim -10$ days since maximum light. Figure 7 shows the resulting bolometric emission from SN 2014C. With $L_{pk} \sim 5 \times 10^{42}$ erg s^{-1}, SN 2014C shows an intermediate peak lumi-

nosity among the sample of well-monitored H-poor SNe of Fig. 7.

In M15 we showed that before the onset of strong SN shock interaction with a massive CSM around $t \sim 100$ days, SN 2014C exhibited typical spectral features of the class of type Ib SNe (i.e. the end points of the evolution of stellar progenitors that managed to shed their hydrogen envelope, while retaining a helium layer). In the absence of strong interaction, the light-curves of SNe that originate from hydrogen-stripped progenitors are powered by the radioactive decay of ^{56}Ni. Specifically, the optical peak luminosity directly reflects the amount of ^{56}Ni produced by the explosion (M_{Ni}), while the light-curve width τ is sensitive to the photon diffusion time scale and thus to the explosion kinetic energy (E_k) and ejecta mass (M_{ej}). We employ the analytical model by Arnett (1982) with the updated formalism by Valenti et al. (2008) and Clocchiatti & Wheeler (1997) to estimate the explosion parameters of SN 2014C.

The spectra acquired around the time of maximum light indicate a photospheric velocity $v_{phot} = 13000 \, \text{km s}^{-1}$ (M15). We use v_{phot} as characteristic velocity v_* of the ejecta to break the degeneracy between M_{ej} and E_k, where[16] $v_* = (10 E_k / 3 M_{ej})^{0.5}$ and assume a constant effective opacity $k_{opt} = 0.07 \, \text{cm}^2 \, \text{g}^{-1}$. Modeling of the bolometric light-curve constrains the time of first light of SN 2014C to 30 December 2013 ± 1 day (MJD 56656 ± 1) and yields the following estimates for the explosion parameters: $M_{Ni} = 0.15 \pm 0.02 \, M_\odot$, $E_k = (1.75 \pm 0.25) \times 10^{51}$ erg, $M_{ej} = 1.7 \pm 0.2 \, M_\odot$. The comparison to the sample of type Ib/c SNe in Fig. 7 leads to the conclusion that the explosion parameters of SN 2014C are typical of the class of SNe with hydrogen-stripped progenitors (Drout et al. 2011, Cano 2013, Lyman et al. 2014).

As a caveat we note that this analytic treatment is sensitive to $k_{opt} M_{ej}$ and $k_{opt} E_k$. As Wheeler et al. (2015) showed, a way to solve for this model degeneracy is by using the late-time light-curve decay slope *under the assumption that it is entirely powered by the radioactive decay of ^{56}Ni and its products*. This assumption does not hold for SN 2014C, which is clearly dominated by interaction at late times, as shown in Fig. 10. For ordinary Ibc SNe Wheeler et al. (2015) find k_{opt} values as low as $0.02 \, \text{cm}^2 \, \text{g}^{-1}$ (e.g. for SN 1994I, their Table 2). For SN 2014C this low value of k_{opt} would imply $E_k \sim 10^{52}$ erg. Energetic SNe with $E_k \sim 10^{52}$ erg are accompanied by broad spectroscopic features that are *not* observed in SN 2014C (M15). We thus conclude that for SN 2014C it is likely that $E_k < 10^{52}$ erg and the effective opacity is $k_{opt} > 0.02 \, \text{cm}^2 \, \text{g}^{-1}$.

In the following we use 30 December, 2013 as explosion date of SN 2014C. The possible presence of a "dark phase" (e.g. Piro & Nakar 2014, 2013) with duration between hours and a few days between the explosion and the time of the first emitted light has no impact on our conclusions.

4. ENVIRONMENT

In this section we employ the knowledge of SN 2014C explosion parameters determined in Sec. 3 and the observables from our broad-band X-ray campaign of Sec. 2 to constrain the density profile of the environment around SN 2014C, shaped by the recent mass-loss history of its progenitor system. The picture that emerges from our analysis, detailed be-

---

[16] We replaced the inaccurate numerical factor given in Eq. 65 of Arnett (1982) with the correct value, as explained in Wheeler et al. (2015).

low, is that of a low-density cavity, with density typical of the environments of ordinary Ibc SNe (e.g. Soderberg 2007), surrounded by a dense shell, with density comparable to the environments of IIn SNe (e.g. Kiewe et al. 2012).

4.1. *Low Density Cavity at $R \lesssim 2 \times 10^{16}$ cm*

At early epochs ($t \lesssim 30$ days), the X-ray emission from SNe originating from H-stripped progenitors is dominated by Inverse Compton (IC) processes (e.g. Björnsson & Fransson 2004). Photospheric optical photons are upscattered to X-ray energies by relativistic electrons accelerated by the SN shock. IC emission depends on the density structure of the SN ejecta, the properties of the explosion, and the characteristics of the medium around the SN (e.g. Chevalier & Fransson 2006).

Following Matzner & McKee (1999), we assume a SN outer density structure $\rho_{SN} \propto R^{-n}$ with $n \sim 9$, as appropriate for stellar explosions arising from compact progenitors. The SN shock accelerates electrons into a power-law distribution $n_e(\gamma) \propto \gamma^{-p}$, where γ is the electron Lorentz factor. Well studied SNe Ib/c indicate $p \sim 3$, with a fraction of post-shock energy into electrons $\epsilon_e \sim 0.1$ (e.g. Chevalier & Fransson 2006). Our modeling of Sec. 3 constrains the explosion kinetic energy $E_k = (1.75 \pm 0.25) \times 10^{51}$ erg and ejecta mass $M_{ej} = 1.7 \pm 0.2 \, M_\odot$, which values we employ here. Finally, the last stages of evolution of massive stars are predicted to be characterized by powerful winds which are expected to shape the immediate SN environment within $R \sim 4 \times 10^{16}$ cm (e.g. Ramirez-Ruiz et al. 2001, Dwarkadas 2007) into a density profile $\rho_{CSM} \propto R^{-2}$.

By employing the IC formalism from Margutti et al. (2012) and the optical bolometric emission from SN 2014C of Sec. 3, we find that the lack of detectable X-ray emission from SN 2014C during the first ~ 20 days (Sec. 2.3) implies a low density environment at distances $R \sim (0.8 - 2) \times 10^{16}$ cm. The inferred mass-loss rate is $\dot{M} < (3 - 7) \times 10^{-6} \, M_\odot \, \text{yr}^{-1}$ for an assumed wind velocity $v_w = 1000 \, \text{km s}^{-1}$. The finding of a low density environment in the proximity of SN 2014C directly constrains the mass-loss history of its progenitor star: in particular, it implies that the progenitor did not suffer massive eruptions within $\Delta t = 7(v_w / 1000 \, \text{km s}^{-1})$ yrs before the final explosion.

4.2. *Region of H-rich Material with Enhanced Density at $R \sim 5.5 \times 10^{16}$ cm*

The rising X-ray and radio luminosity of the type Ib SN 2014C at late times, coupled with the progressive emergence of prominent Hα emission (Fig. 10), clearly suggests a scenario where the freely expanding, H-poor SN 2014C ejecta encountered a dense H-rich region in the proximity of the explosion site. We constrain the properties of the H-rich, dense CSM shell by using the following observables:

- Optical spectroscopy that we presented in M15 constrains the emergence of Hα emission due to the interaction of the SN ejecta with H-rich material in the CSM to $t > 30$ days. A prominent Hα profile has developed by day 130 after the explosion. In the following we use $t = 130$ days as the start time of the *strong* CSM interaction.

- The broad-band X-ray luminosity shows a sharp rise during the first ~ 300 days and reaches its maximum value $L_x \sim 5 \times 10^{40} \, \text{erg s}^{-1}$ by ~ 500 days.

- The X-ray emission is of thermal origin and the observed temperature is $T \sim 20$ keV between 400 and 500 days after the explosion.

- There is significant evidence for decreasing absorption with time, with NH_{tot} evolving from $\sim 4 \times 10^{22}$ cm^2 at ~ 300 days, to $\sim 2 \times 10^{22}$ cm^2 at ~ 500 days after the explosion.

The interaction of freely expanding SN ejecta with the CSM leads to the formation of a double shock interface layer, with the forward shock (FS) propagating into the CSM and the reverse shock (RS) decelerating the SN ejecta. For the SN ejecta we adopt a power-law density distribution with $\rho_{SN} = \rho_0 (v/v_0)^{-n}$ for $v > v_0$ and $\rho_{SN} = \rho_0$ for ejecta velocities $v < v_0$. For the explosion parameters of SN 2014C the transitional velocity is $v_0 \sim 10700$ km s^{-1}. We assume $n = 9$ as appropriate for compact stellar progenitors (Matzner & McKee 1999). We follow Chevalier (1982) to describe the dynamics of the shock propagation into the low density bubble, and Chevalier & Liang (1989) to compute the dynamics of the strong interaction of the SN ejecta with the dense shell.

4.2.1. Expansion in the Bubble

The dynamics of the double shock structure that originates from the interaction of the outer power-law portion of the SN ejecta profile with a wind-like CSM with density $\rho_{CSM} = \dot{M}/(4\pi v_w R^2)$ is described by a self-similar solution (Chevalier 1982). From Sec. 4.1, $\dot{M} < (3-7) \times 10^{-6}$ M$_\odot$ yr^{-1} for $v_w = 1000$ km s^{-1}. With these parameters, we find that the FS radius at the time of the start of the strong interaction ($t = 130$ days) is $\sim 5.5 \times 10^{16}$ cm. The swept up mass of gas within the bubble is $M_{bubble} < 10^{-4}$ M$_\odot$. M_{bubble} is considerably smaller than the mass in the outer power-law section of the SN ejecta ($M_{ej,PL} \sim 0.6$ M$_\odot$), which is thus only minimally decelerated during its expansion into the cavity. The velocity of the FS just before the start of the strong interaction is ~ 44000 km s^{-1}. The CSM density at the outer edge of the bubble is < 100 cm^{-3}.

4.2.2. Interaction with the dense, H-rich CSM

The rising X-ray and radio luminosity with time is suggestive of a large density contrast between the bubble and the shell of dense CSM at $R_{shell} \sim 5.5 \times 10^{16}$ cm, as confirmed by our modeling below. Under these circumstances (i.e. $\rho_{bubble} \ll \rho_{shell}$ and $M_{ej,PL} \gg M_{bubble}$), the outer density profile of the SN ejecta continues to interact with the dense shell of CSM and the energy transmitted to the shell is initially modest (Chevalier & Liang 1989). The analysis by Chevalier & Liang (1989) shows that the flow once again has a self-similar nature, with $R_{RS} = 0.92 R_{shell}$ for $n = 9$ (their Table 2).

The collision of the SN ejecta with the dense CSM shell causes a sudden increase of the X-ray luminosity of both the RS and the FS (see e.g. Chugai & Chevalier 2006, their Fig. 2). The FS experiences rapid deceleration, with v_{FS} decreasing from ~ 44000 km s^{-1} to a $\sim$ few 1000 km s^{-1}, as suggested by the measured width of the intermediate component of the Hα line in our spectra, which maps the dynamics of the shocked, H-rich CSM shell (Fig. 10, M15). Since the velocity of the shock determines the energy imparted to particles that cross the shock, the characteristic temperature of emission of material in the FS plummets: contrary to the previous phase of

expansion within the bubble, the interaction with a wall of material causes the FS temperature to be significantly below the temperature of the RS. During the expansion in a wind-like medium $T_{RS}/T_{FS} \propto v_{RS}^2/v_{FS}^2$ or $T_{RS} \propto T_{FS}/(n-3)^2 \sim 0.03 T_{FS}$ for $n = 9$, see e.g. Chevalier & Fransson (2003).

This rapid deceleration is followed by a period of steady acceleration as the faster SN ejecta piles up from behind (Chevalier & Liang 1989, Dwarkadas 2005). The radius of the shock wave expands as $R_{FS} = R_{shell} + K_1(A R_{shell}^{2-n} t^{n-3}/\rho_{shell})^{1/2}$, where $K_1 = 0.26$ for a nonradiative shock and $K_1 = 0.24$ for a radiative shock front, $n = 9$, $A \equiv A(E_k, M_{ej}, n)$ and we have assumed a smooth CSM shell with density ρ_{shell} (Chevalier 1984, Chevalier & Liang 1989).

We proceed within the "thin shell" approximation (e.g. Chevalier 1982), where the shocked gas, made by shocked CSM *and* shocked SN ejecta, can be treated as a thin shell with mass M_s, radius $R_s(t)$ and velocity $v_s(t)$. $v_{FS} \approx v_s$, the velocity of the (unshocked) ejecta at the RS is $v_{SN} = R_s/t$ and $v_{RS} \approx v_{SN} - v_{FS}$. For a decelerated FS velocity $v_{FS} \approx$ a few 1000 km s^{-1}, we estimate at $t \sim 400$ days $R_s \sim 6 \times 10^{16}$ cm and $v_{RS} \sim 13000$ km s^{-1}. The RS temperature is directly connected to its velocity by $T_{RS} = 2.27 \times 10^9 \mu_p v_{RS,4}^2$, where $v_{RS,4} \equiv v_{RS}/10^4$ km s^{-1} and μ_p is the mean mass per particle including electrons and ions (e.g. Fransson et al. 1996). We follow Chugai & Chevalier (2006) and approximate the shocked SN ejecta by a mixture of 65% He, 33% O and 2% Fe by mass. For this composition of the ejecta and complete ionization, $\mu_p = 1.33$ and $T_{RS} > 400$ keV, which is much larger than the $T \sim 18$ keV indicated by our broad-band X-ray spectral analysis (incomplete ionization would lead to even larger temperatures). This finding thus suggests that the detected X-ray emission is dominated by the FS. Under this hypothesis, $T_{FS} = 18$ keV at $t \sim 400$ days, which implies $v_{FS} \sim 4000$ km s^{-1}, consistent with the indication of $v_{FS} \sim$ few 1000 km s^{-1} from the optical spectra. Solar abundances have been assumed for the CSM (i.e. $\mu_p = 0.61$).

The mass of the shocked CSM material is directly constrained by the observed bremsstrahlung spectrum. The observed X-rays at $t \sim 500$ days, with $T \sim 20$ keV and $L_x \sim 5 \times 10^{40}$ erg s^{-1} require an emission measure $EM_{FS} \sim 1.4 \times 10^{63}$ cm^{-3}, where $EM \equiv \int n_e n_I dV$. Accounting for the presence of an additional thermal component of emission from the RS at $T \gg 20$ keV reduces the required EM to $EM_{FS} \sim 1.1 \times 10^{63}$ cm^{-3} and suggests $EM_{RS} \sim 4.3 \times 10^{62}$ cm^{-3}. To estimate the mass of the shocked CSM gas we need to constrain the volume of the shocked CSM. Interpreting the occurrence of the peak of the emission at $t \sim 500$ days as due to the passage of the shock front through the CS shell, we constrain the shell thickness $\Delta R_{shell} \sim 10^{16}$ cm. The mass of the shocked CSM is thus $M_{CSM} \sim (1.0 - 1.5)$ M$_\odot$ with density $\rho_{shell} \sim 2 \times 10^6$ cm^{-3}. Introducing a volume filling factor f defined as $V_{shell} = 4\pi R_{shell}^2 \Delta R_{shell} f$, the previous estimates would scale as:$M_{CSM} \propto f^{1/2}$ and $\rho_{shell} \propto f^{-1/2}$.

The volume of the reverse postshock layer between the reverse shock and the contact surface can be easily computed considering that for $n = 9$, $R_{RS} = 0.92 R_{shell}$ (Chevalier & Liang 1989). For $EM_{RS} \sim 4.3 \times 10^{62}$ cm^{-3} the mass of the shocked SN ejecta is thus $M_{ej,RS} \sim 0.7$ M$_\odot$. As a sanity check we note that momentum conservation implies that the mass of the CSM required to decelerate ~ 0.7 M$_\odot$ of SN ejecta with typical velocity $(2E_k/M_{ej})^{1/2} \gtrsim 10^4$ km s^{-1} down to ~ 4000 km s^{-1} is $M_{shell} \gtrsim 1.4 M_{ej,RS}$ or $M_{shell} \gtrsim 1$ M$_\odot$, consistent with our esti-

mates above.

From another perspective, since the observed emission is dominated by the FS, the detected decrease of X-ray absorption with time (Fig. 4) provides an independent constraint to the amount of neutral CSM material in front of the FS.[17] The detected temporal variation of NH_{tot} directly implies that the material responsible for the absorption is local to the SN explosion and within the reach of the SN shock over the time scale of our observations. From $t = 308$ days to 472 days after the explosion we measure $\Delta NH_{tot} \sim 2 \times 10^{22}\,cm^{-2}$. For $v_{FS} \sim 4000\,km\,s^{-1}$, the detected ΔNH_{tot} constrains the neutral CSM mass probed by the shock front between 308 days and 472 days to be $M_{CSM,NH} \sim 0.6\,M_\odot$, while the total CSM shell mass is $\gtrsim 1.2\,M_\odot$, assuming that the FS did not experience substantial acceleration and the CSM shell is spherical and homogeneous.

Finally, while a detailed hydrodynamical simulation is beyond the scope of the present work, we end the section emphasizing the qualitative agreement of our conclusions, derived from a purely analytical treatment, with the results from the simulations from Chugai & Chevalier (2006). In order to reproduce the properties of SN 2001em, Chugai & Chevalier (2006) simulated the collision of freely expanding SN Ibc ejecta with a dense shell of H-rich material at $R_{shell} = (5-6) \times 10^{16}\,cm$ with thickness $\Delta R_{shell} \sim 10^{16}\,cm$ and $M_{shell} = (2-3)\,M_\odot$. The simulation thus differs from our situation only in terms of the larger mass of the CSM shell. These authors find that the SN ejecta interaction with the dense medium causes a large increase of L_x of both shocks, with L_x reaching $L_x \sim 10^{41}\,erg\,s^{-1}$ at peak. The FS, which was hotter than the RS before the strong interaction, experiences rapid deceleration, followed by a period of acceleration until the shock front reaches the edge of the shell. As a result, $T_{FS} \ll T_{RS}$ after the interaction (e.g. at $t = 1000$ days, $T_{FS} \sim 5$ keV and $T_{RS} \sim 100$ keV, and $T_{RS} \sim 850$ keV at $t = 500$ days, see their Fig. 2). Compared to SN 2014C, the FS in the simulations by Chugai & Chevalier (2006) is more strongly decelerated by the impact with the CSM shell, due to the larger mass of the shell (the SN ejecta parameters are instead comparable). For the same reason, in their simulations the peak of the X-ray emission due to the passage of the shock front through the CSM shell is also delayed with respect to SN 2014C (~ 1000 days, vs. ~ 500 days). Apart from these *expected* differences, our analytical treatment captures the key physical properties of the SN ejecta- CSM strong interaction.

4.2.3. *Anticipated Evolution at Later Times*

The shock acceleration phase, caused by the increase of the pressure in the shocked region due to the interaction with the outer density profile of the SN ejecta, ends when (i) the RS reaches the flat portion of the ejecta profile; or (ii) the energy transmitted to the CSM shell becomes large compared to the energy of the shocked ejecta; or, alternatively, (iii) the shock front reaches the edge of the CSM shell (Chevalier & Liang 1989).

The time scale at which the RS reaches the bend in the SN ejecta profile is $t_1 \sim R_{RS}/v_0$, where $v_0 \equiv v_0(E_k, M_{ej}, n)$ is the transitional velocity that defines the SN ejecta profile and $v_0 \sim 10700\,km\,s^{-1}$ for the explosion parameters of SN 2014C. Following Chevalier & Liang (1989), $t_1 \sim (R_{shell}/v_0)(1 + 3\gamma(\gamma -$

$1)/((\gamma+1)(n-5)))^{-1/3} \approx 0.92(R_{shell}/v_0)$ for $n = 9$ and an adiabatic index $\gamma = 5/3$. For SN 2014C we thus derive $t_1 \gtrsim 550$ days.

The time scale t_2 at which the energy transferred to the CSM gas is ≥ 0.5 the total energy in the shocked region depends on the explosion parameters and on the properties of the CSM shell $t_2 \equiv t_2(M_{ej}, E_k, n, \rho_{shell}, R_{shell})$. Employing the formalism by Chevalier & Liang (1989), their Eq. 3.24, we find $t_2 > 550$ days for $\rho_{shell} \geq 4 \times 10^6\,cm^{-3}$.

L_x reaches its maximum at $t < 500$ days (Fig. 6), from which we deduce that the shock front already reached the edge of the high-density region by $t_3 \sim 500$ days. The later dynamics of the interaction is thus likely determined by this event, even if the time scales t_1 and t_2 are close enough that a simulation is needed to capture the details of the evolution.

Once the shock has transversed the dense shell, a rarefaction wave propagates into the interaction region, while the FS expands into a less dense medium that was shaped by the previous phase of evolution of the progenitor of SN 2014C. The simulations by Chugai & Chevalier (2006) show that the X-ray luminosity remains high even after the shell has been overtaken, but that the temperature of emission of both shocks declines with time. According to our calculations, for SN 2014C, the temperature of the RS shock will enter the NuSTAR passband at $t > 800$ days ($T_{RS} \sim 100$ keV at $t \sim 800-1000$ days, depending on the ionization state of the ejecta). Future observations will allow us to sample the density of the CSM outside the dense shell. At the moment we note that optical spectroscopy of SN 2014C (M15) reveals that the material outside the CSM shell is H-rich and shows velocities $< 100\,km\,s^{-1}$ (from the narrow component of the Hα line, Fig. 10). These velocities are typical of winds emanating from non-compact progenitors, and are typically associated with the large mass-loss rates (and densities) inferred for type IIn SNe (e.g. Kiewe et al. 2012). It is thus possible that the shocked gas will never re-enter a phase of free expansion.

4.2.4. *Clumpy Structure of the CSM*

Two independent sets of observations point to a complex structure of the interaction region with overdense clumps of emitting material: (i) the velocity profile of the shocked H-rich material; (ii) the presence of prominent Fe emission lines in the X-ray spectra.

The progressive emergence of an Hα emission (Fig. 10) indicates the presence of shocked H-rich CSM. However, optical spectroscopy in Fig. 10 (see M15 for details) shows velocities $< 2000\,km\,s^{-1}$ for the shocked material, while above we infer $v_{FS} \sim 4000\,km\,s^{-1}$ for the expansion of the shock front at the same epoch. These two results can be reconciled if the H-rich material that dominates the Hα emission is clumpy and is concentrated in regions with density contrast $\rho_{clumps}/\rho_{shell} \approx 4$.

Astrophysical plasmas with $T < 3 \times 10^7$ K produce a forest of X-ray lines. At higher temperatures line emission is inhibited and cooling is dominated by bremsstrahlung. At $T \sim 20$ keV (i.e. $\sim 2 \times 10^8$ K) the only transitions that survive are those associated with extremely ionized states of Fe atoms, i.e. He-like and H-like Fe atoms. Consistent with these expectations, in each epoch of observation we clearly identify a localized excess of X-ray emission at $\sim 6.7-6.9$ keV that we associate with He-like and H-like Fe atoms transitions (Fig. 4 and 5). However, a single-temperature, collisionally-ionized plasma model in thermal equilibrium fails to reproduce the

observed luminosity of the Fe emission at all epochs. At temperature ~ 20 keV and density $\sim 4 \times 10^6\,\mathrm{cm}^{-3}$ the time for electrons and protons to come into equilibrium is $t_{ei} < t_{obs}$ and $t_{ei} \sim 80$ days (Spitzer 1962), justifying our assumption of thermal equilibrium so far. The only way to reconcile the prominent Fe emission within this model is to invoke extremely super solar abundances (~ 5 times the solar value) for the shocked CSM shell. Alternatively, observations are consistent with a multi-phase plasma, with a lower temperature (and higher density) component responsible for the Fe emission. Given the independent suggestion of a clumpy medium from the Hα velocity profile, we consider this second possibility of a medium with components of different densities (and not necessarily spherically simmetric) more likely.

Evidence or hints for an excess of emission around $6.7-6.9$ keV has been found in some SNe characterized by strong interaction with a dense medium. Examples include the type-IIn SNe 1996cr (Dwarkadas et al. 2010, Dewey et al. 2011), 2006jd (Chandra et al. 2012) and SN 2009ip (Margutti et al. 2014a). In all cases the excess has been interpreted as originating from H- and He-like transitions of collisionally ionized Fe atoms. Interestingly, in the case of SN 2006jd, Chandra et al. 2012 arrived to a similar conclusion of either a very enriched medium with super solar abundances or a multi-phase plasma to explain the luminous Fe emission.

5. SN2014C IN THE CONTEXT OF 183 IB/C SNE WITH RADIO OBSERVATIONS

5.1. *Rate of 14C-like explosions among Ib/c SNe*

The metamorphosis of SN 2014C from an ordinary type-Ib SN into a strongly interacting SN of type IIn over a time scale of ~ 1 yr is signaled by the progressive emergence of Hα emission and narrow line emission in the optical/UV band, accompanied by a marked increase of both the radio and X-ray emission produced by the SN shock interaction with a "wall" of dense H-rich material presumably deposited in the environment by the stellar progenitor before death (Fig. 10). In this section we quantify how common this phenomenology is among SNe originating from H-stripped stars by using the available set of published data from radio monitoring campaigns of type Ib/c SNe. We focus on the radio wavelength range as it offers the most homogeneous data set with observations covering the early- and late-time evolution of Ib/c SNe.

Our sample comprises public observations of 183 type Ib/c SNe obtained over more than 20 years of radio monitoring campaigns, with data acquired from a few days to ~ 32 yrs since the SN explosion. The data have been collected from Berger et al. (2003), Soderberg et al. (2006), Soderberg (2007), Bietenholz et al. (2014), Corsi et al. (2014), Kamble et al. (2014), Drout et al. (2015) and references therein. In 41 cases the radio observations provide meaningful constraints to the presence of a 14C-like radio re-brightening (i.e. the observations are deep enough and cover the late-time evolution of the transient at $t \gtrsim 500$ days). For the remaining 142 SNe Ib/c the available observations do not typically reach the necessary depth and/or do not extend to late times.

Out of 41 type Ib/c SNe with good radio coverage, we can rule out a 14C-like radio re-brightening in 37 cases. For the type Ib/c SNe 2001em (Bietenholz & Bartel 2005, Schinzel et al. 2009), 2003gk (Bietenholz et al. 2014), 2007bg (Soderberg 2007, Salas et al. 2013) and PTF11qcj (Corsi et al. 2014) we find evidence for late-time, luminous radio re-brightenings consistent with a 14C-like phenomenology. In particular we

note that (i) albeit sparsely sampled, the X-ray and optical evolution of the type-Ic SN 2001em (Filippenko & Chornock 2001) are also reminiscent of SN 2014C (Chugai & Chevalier 2006); (ii) we further point out the possible detection of an outburst from the stellar progenitor of PTF11qcj ~ 2.5 yrs before the explosion (Corsi et al. 2014). We thus conclude that $\sim 10\%$ of Ib/c SNe with constraining radio observations displays late-time radio re-brigtenings reminiscent of SN 2014C and that, when available, multi-wavelength observations of this subset of SNe independently support the idea of an enhanced mass loss from the progenitor star during the last stages of evolution preceding core collapse. We note that while this sample has been collected from different sources, there is no obvious observational bias that would favor a larger fraction of interacting systems. In fact, radio SNe tend to be followed up at later times in the case of an early time radio detection, which suggests that we might have missed later time radio re-brightenings in systems with faint or undetected early emission. This source of bias is alleviated in part by the fact that some SNe in our sample have been followed up at early and late times (irrespective from a detection of lack thereof) as part of the searches for off-axis emission from a Gamma-Ray Burst-like jet. We quantify this source of uncertainty in the next paragraph.[18]

Figure 8 summarizes the results from the analysis of the enlarged sample of 60 Ib/c SNe for which constraining radio observations have been obtained at some time since the explosion (i.e. we relaxed the condition of a radio monitoring extending to late times $t \gtrsim 500$ days of the previous paragraph). This plot shows that existing radio observations rule out the presence of strong interaction in a large fraction of Ib/c SNe *only* at early times (e.g. for $t \lesssim 100$ days, $\gtrsim 80\%$ of Ib/c SNe do not show evidence for strong shock interaction), while at later times the phase space is sparsely sampled, so that, for example, we can exclude a 14C-like behavior at $t \gtrsim 1000$ days only for $\sim 40\%$ of the SNe.

Finally we note that SN 2014C represents an extreme case of radio flux variability. Small-scale radio light-curve modulations at the level of a factor ~ 2 in flux are common and found in $\sim 50\%$ of SNe Ib/c with radio detection (see also Soderberg 2007). This phenomenology can be explained within the context of turbulence-driven small-scale clumping of the stellar wind (Moffat 2008), a physical process that generates moderate density variations of a factor $\sim 2-4$ in the stellar environment. The "bubble plus thick shell structure" that we infer for SN 2014C clearly demands a different origin. More pronounced achromatic radio flux variations due to modulations of the environment density of a factor $\sim 3-6$ have been observed in SNe 2004cc, 2004dk and 2004gq (Wellons et al. 2012). In particular, the radio light-curve of SN 2004cc shows a well-defined double-peaked structure with flux contrast ~ 10, a first peak of emission at ~ 25 days and a second radio peak at ~ 150 days since explosion (Wellons et al. 2012, their Fig. 1). While this behavior is somewhat reminiscent of SN 2014C, the radio flux from SN 2004cc rapidly and significantly faded on a timescale $\Delta t/t \lesssim 1$, pointing to a smaller mass of the dense region encountered by the SN shock. This comparison highlights the

---

[18] We also would like to mention the existence of SNe (e.g. SNe 1986J and 1996cr, Rupen et al. 1987, Dwarkadas et al. 2010) that have been discovered at late times from their bright radio emission and classified as type IIn events from their late-time spectra. These events are not part of this sample by definition. However, we note that they might have been classified as type Ib/c SNe if early optical spectra had been available.
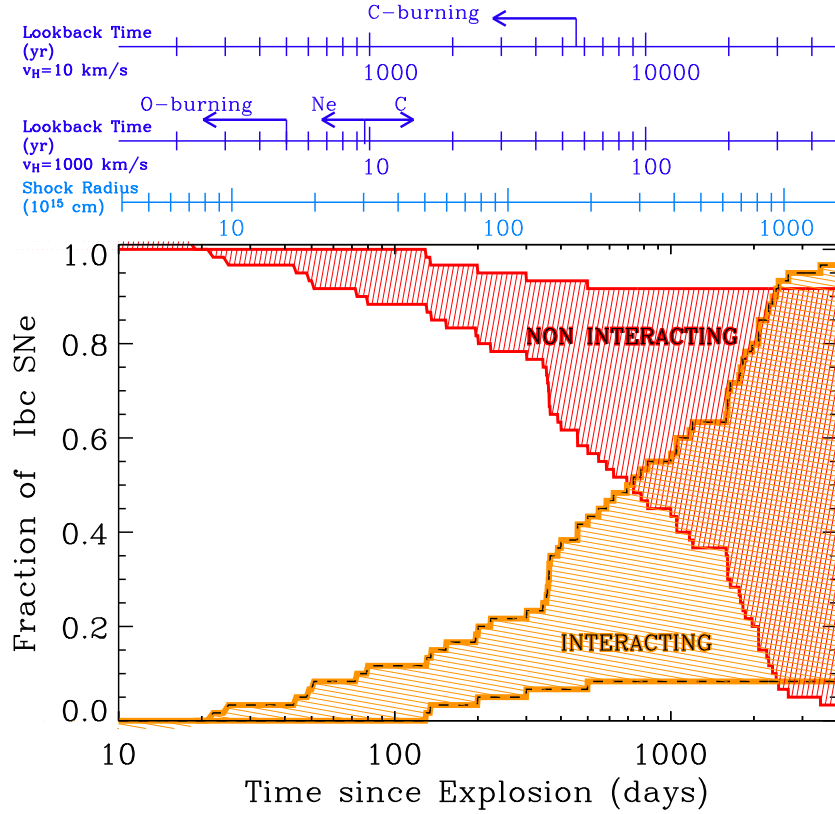
FIG. 8.— Constraints to the fraction of Ib/c SNe that are interacting (orange shaded area) or non interacting (red shaded area) with a 14C-like medium as a function of time since the explosion, as derived from the analysis of 60 SNe of type Ib/c with constraining radio observations. For this sample, the fraction of objects that does not show signs of interaction at very early times is 100% by definition, as we selected spectroscopically classified type Ib/c SNe (SNe with signs of interaction since the very first moment would be instead classified as IIn or Ibn events depending on the H-rich or He-rich composition of the medium, respectively) The time since the explosion is converted into a shock radius by employing a standard shock velocity of $0.15c$. We show the lookback time for two representative ejection velocities of the H-rich material v_H. The corresponding nuclear burning stages are for a non-rotating stellar progenitor of $12 \, M_\odot$ with solar metallicity from Shiode & Quataert (2014).
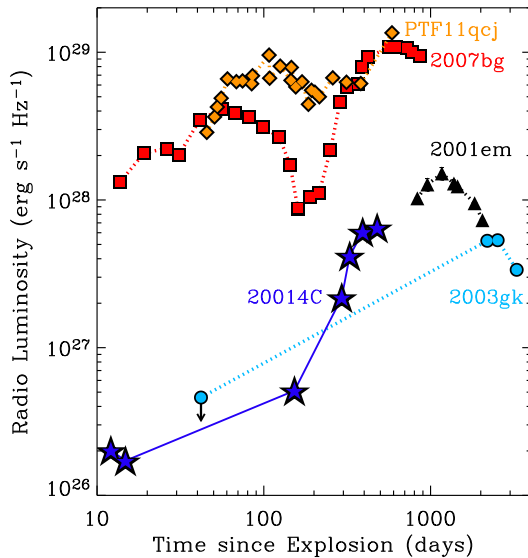

FIG. 9.— The type Ib/c SNe 2001em, 2003gk, 2007bg and PTF11qcj display late-time radio re-brightenings with similarities to SN 2014C. 8.5 GHz data have been shown for SNe 2001em, 2003gk and 2007bg (Schinzel et al. 2009, Bietenholz et al. 2014, Salas et al. 2013). For PTF11qcj we show here the 7.4 GHz data from Corsi et al. (2014). For SN 2014C we use observations acquired at 7.1 GHz (K15).

fact that, among type Ib/c SNe, 14C-like events might represent the most extreme manifestations of a more common physical process that induces severe progenitor mass loss synchronized with the final explosion on a variety of mass-loss scales. With this notion in mind, in the following we concentrate on the nature of 14C-like SNe.

5.2. *Statistical inference on the nature of the underlying physical process*

Current radio studies efficiently sample the first $t \sim 500$ days of evolution of Ib/c SNe (Fig. 8). The direct implication is that for a typical SN shock velocity of $\sim 0.15c$ we are currently systematically exploring a region of $\sim 2 \times 10^{17}$ cm around Ib/c SNe. For a medium that has been enriched by material ejected by the stellar progenitor with velocity v_w, this fact implies that we are effectively sampling $\Delta t_{sampled} \sim 60 \times (v_w/1000 \, \mathrm{km \, s^{-1}})^{-1}$ yrs of life of the massive progenitor star before the explosion. This value corresponds to a very small fraction $f < 2 \times 10^{-3}$ of the entire life span τ of a massive star, even in the case of slowly moving material with $v_w = 10 \, \mathrm{km \, s^{-1}}$ and a very massive progenitor with a short life of $\tau \sim 3$ Myrs. We consider $v_w = 10 - 1000 \, \mathrm{km \, s^{-1}}$ a representative range of velocities of the ejected material. Velocities of the order of $v_w \sim 10 \, \mathrm{km \, s^{-1}}$ are expected in the case of common envelope ejection by a binary system, while $v_w \sim 1000 \, \mathrm{km \, s^{-1}}$ are the typical wind velocities observed in Wolf-Rayet stars.

From Sec. 5.1, the fraction of 14C-like objects is $\gg f$, which implies that 14C-like mass ejections preferentially occur towards the end of the life of the stellar progenitor. We will refer to the interval of stellar lifetime during which a mass ejection can occur as the progenitor "active time" (Δt_{active}). The physical process responsible for the mass ejection is thus closely synchronized with the stellar death.

The results from Sec. 5.1 are statistically consistent with two scenarios. (i) We are sampling a representative portion of Δt_{active} of Ib/c SN progenitors and $\Delta t_{active} \sim \Delta t_{sampled}$. Mass ejections are intrinsically rare and only happen in a limited fraction ($\sim 10\%$) of progenitors under peculiar circumstances. (ii) $\Delta t_{active} \gg \Delta t_{sampled}$, all Ib/c SN progenitor stars experience an active phase and the small sample of Ib/c SNe with evidence for strong interaction is a mere consequence of our incomplete sampling of the previous stages of stellar evolution. If this is the case $\Delta t_{active} \sim 500 \times (v_w/1000\,\mathrm{km\,s^{-1}})$ yrs. The minimum and maximum Δt_{active} consistent with the detection of 4 strong radio re-brigthenings out of a sample of 41 Ib/c SNe can be easily derived from a binomial distribution with $p = \Delta t_{sampled}/\Delta t_{active}$, where p is the probability of success (e.g. Romano et al. 2014). For $v_w = 1000\,\mathrm{km\,s^{-1}}$ we find $200\,\mathrm{yr} < \Delta t_{active} < 5000\,\mathrm{yr}$ (3σ confidence level), while for $v = 10\,\mathrm{km\,s^{-1}}$ we find $22000\,\mathrm{yr} < \Delta t_{active} < 500000\,\mathrm{yr}$.

We consider hypothesis (ii) the most likely scenario, since we are only sampling a limited portion of the parameter space and we have no reasons to believe that the portion that we are sampling is truly representative of the entire distribution.

6. INTERPRETATION AND DISCUSSION: MASSIVE STAR EVOLUTION REVISED

6.1. *A continuum of stellar explosions between type Ib/c and type-IIn SNe*

SN 2014C experienced a remarkable metamorphosis, evolving from an *ordinary* type-Ib SN to a strongly interacting type-IIn SN over the time scale of ~ 1 yr. Figure 10 captures the key observational properties of its evolution over the electromagnetic spectrum: radio, X-ray and Hα emission progressively got stronger with time, while the optical light-curve flattened, due to the contribution from the SN shock interaction with dense material in the environment. The strong interaction of the SN shock with a dense, H-rich material is the defining property of SNe of type IIn. In this sense, SN 2014C bridges the gap between type Ib/c and type IIn SNe (Fig. 11). We showed in Sec. 4 that this phenomenology requires the deposition of a substantial amount of H-rich material ($\sim 1\,\mathrm{M_\odot}$) in the SN surroundings at $R \sim 5.5 \times 10^{16}$ cm.

The low density environment at $R \lesssim 2 \times 10^{16}$ cm (Sec. 4.1) implies that the progenitor star of SN 2014C did not suffer massive eruptions within $\sim 7(v_w/1000\,\mathrm{km\,s^{-1}})$ yrs before death. The location of the dense H-rich shell at $R \sim 5.5 \times 10^{16}$ cm argues for an ejection of H-rich material at an earlier epoch corresponding to $\sim 20(v_H/1000\,\mathrm{km\,s^{-1}})$ yrs preceding the explosion, where v_H is the ejection velocity of the shell. For SN 2014C, the H-rich shell was far enough from the explosion site not to be efficiently ionized by the SN shock and radiation during the first ~ 100 days -which allowed the early SN classification as an H-poor, type Ib event-, but close enough for the shock-CSM interaction to develop on time scales that are relevant to our coordinated monitoring -which allowed us to witness the later transition to type IIn SN- (Fig. 11).

A key difference between ordinary IIn SNe and 14C-like events lies in the location of the H-rich material, which maps into a different epoch of H-envelope ejection by the stellar progenitors. Ordinary type IIn SNe are characterized by strong interaction with dense CSM since the very first moments after explosion, which requires a very recent ejection of the H-rich material (typically within a few years before the stellar demise) and results in the H-rich material being at $R < 10^{16}$ cm from the explosion center.

Recent observations indeed provided direct evidence for eruptive behavior of progenitors of type IIn-like SNe in the years to days before a major explosion (Smith 2014). Our observations of SN 2014C suggest that a fraction of SNe spectroscopically classified of type IIn in fact contained bare type Ib/c-like cores that recently ejected their H envelopes. This suggestion would naturally account for the diverse environments of IIn SNe (which argue for a broad range of progenitor star masses; Kelly & Kirshner 2012, Anderson et al. 2015) and it is in line with what was inferred for the type-IIn SN 1996cr (Dwarkadas et al. 2010). In general, our picture would explain the observational properties of type-IIn SNe like 1986J that did not show evidence for high-velocity H features during its spectroscopic evolution, but showed evidence for broad O features at late times (Rupen et al. 1987, Bietenholz et al. 2002, Milisavljevic et al. 2008).

Previous studies pointed to a continuum of properties among SNe interacting with He-rich and H-rich material (i.e. type-Ibn SNe and SNe of type IIn, Smith et al. 2012, Pastorello et al. 2015 and references therein). With our study we significantly extend the continuum to include even H-stripped core-collapse explosions. The existence of 14C-like events argues in favor of a continuum of stellar explosions that bridges the gap between Ib/c and IIn SNe (Fig. 11) and that directly maps into a continuum of time scales of ejection of the H-rich envelope of progenitors of H-stripped SNe, extending from less than one year to thousands of years before explosion.

6.2. *The origin of the H-rich shell in SN 2014C*

SN 2014C is an ordinary type Ib/c SN embedded in a non-standard H-rich environment shaped by the mass-loss history of its progenitor system. Here we discuss the origin of the H-rich, dense CSM material around SN 2014C in the context of the stellar evolution and mass-loss mechanisms of evolved massive stars.

Single massive stars that are progenitors of ordinary H-stripped SNe are expected to evolve from H-rich, extended Red SuperGiants (RSGs) into core-He-burning compact Wolf-Rayet (WR) stars $\sim 0.5-1$ Myr before exploding as H-poor SNe (e.g. Heger et al. 2003). The presence of H-rich material within $\sim 6 \times 10^{16}$ cm of the explosion site of SN 2014C demands an exceptionally short WR phase of its progenitor star, lasting only ~ 20 yrs (for an ejection velocity of the H-rich material $v_H = 1000\,\mathrm{km\,s^{-1}}$), and a very large mass-loss rate during the previous RSG phase $\dot{M}_{RSG} \geq 2 \times 10^{-3}\,\mathrm{M_\odot\,yr^{-1}}$ (the inequality accounts for the fact that the RSG wind is in fact freely expanding). This value is ≥ 10 times larger than the typically observed mass-loss rates during the RSG phase (observations indicate $\dot{M}_{RSG} < 10^{-4}\,\mathrm{M_\odot\,yr^{-1}}$, van Loon et al. 2005, Mauron & Josselin 2011) and exceeds the limit for mass loss due to the commonly assumed line-driven winds even in the case of a small filling factor $f = 0.1$ of the H-rich shell (e.g. Smith 2014, their Fig. 3).[19]

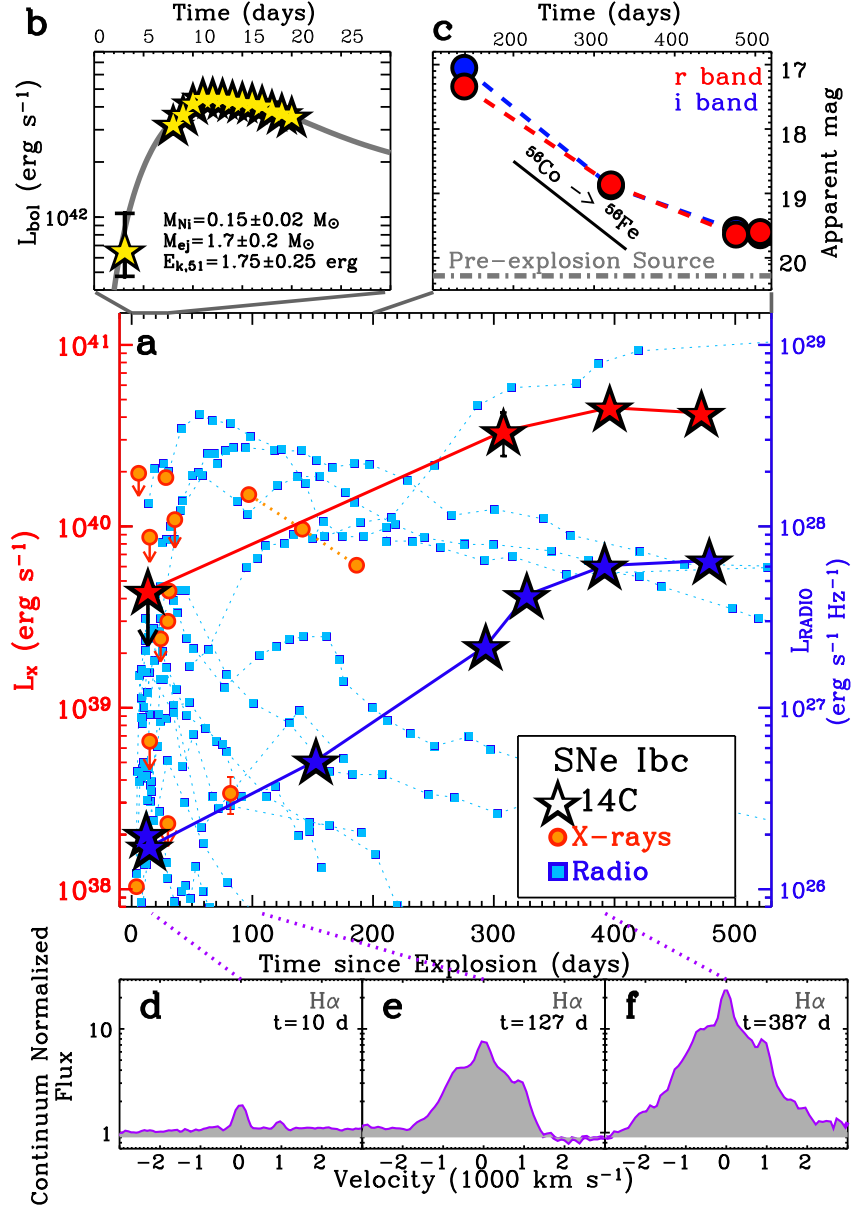[19] Another possibility is that SN 2014C exploded in an environment en-

FIG. 10.— This plot summarizes the key and unique observational features of SN 2014C over the electromagnetic spectrum. *Central Panel:* X-ray (red stars) and radio (7.1 GHz, blue stars) evolution of SN 2014C compared to a sample of Ibc SNe from Margutti et al. (2014b) and Soderberg et al. (2010). SN 2014C shows an uncommon, steady increase in X-ray and radio luminosities until late times, a signature of the continued shock interaction with very dense material in the environment. *Upper panels*: The optical bolometric luminosity of SN 2014C is well explained at early times by a model where the source of energy is purely provided by the radioactive decay of ^{56}Ni (grey thick line, top left panel). However, at later times (top right panel) SN 2014C shows a significantly flatter temporal decay, due to the contribution of more efficient conversion of shock kinetic energy into radiation. This evolution is accompanied by a marked increase of Hα emission (*Lower Panels*), as a consequence of the SN shock interaction with H-rich material. See M15 and K15 for details about the spectroscopical metamorphosis and the radio evolution, respectively.
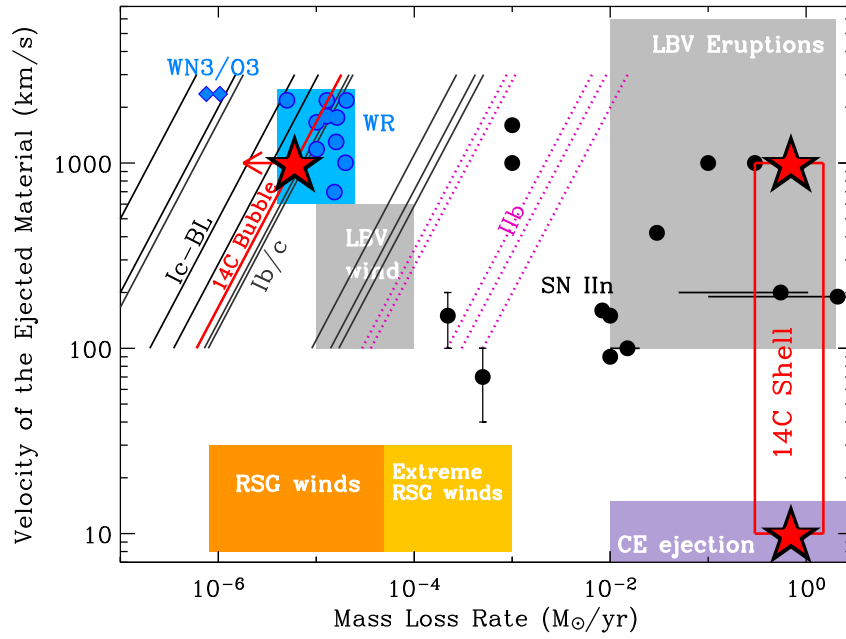
FIG. 11.— The environment sampled by the SN 2014C shock evolves from the typical low-density environment around Ib/c SNe and WR stars, to the dense and rich environment typical of SNe that develop signatures of strong interaction with the medium (i.e. type-IIn SNe, here represented with black dots, data from Kiewe et al. 2012). H-poor SNe are represented with diagonal lines since the observations constrain the density ρ which is $\propto \dot{M}/v_w$. Black, blue and dotted purple lines are used for the sample of type Ic-BL, Ib/c/ and IIb SNe from Drout et al. 2015. The properties of galactic WR stars are from Crowther (2007), while WN3/O3 stars are from Massey et al. (2015). Locations of red supergiants environments (RSG) are from de Jager et al. (1988), Marshall et al. (2004) and van Loon et al. (2005), while the typical locations of Luminous Blue Variable (LBV) winds and eruptions are inferred from Smith (2014) and Smith & Owocki (2006). For the common envelope (CE) ejection due to binary interaction we use here a typical time scale of 1 yr.

We thus conclude that SN 2014C violates several expectations from standard evolutionary models that employ time averaged mass-loss prescriptions and do not include highly time-dependent mass-loss episodes associated with instabilities during the last stages of stellar evolution and the effects of binarity. With SN 2014C we further have clear evidence that mass-loss mechanisms other than the commonly-assumed metallicity-dependent line-driven winds are active and play an important role in the process that leads to the H-stripped progenitors of SNe Ib/c. This picture, if common among Ib/c SN progenitors, naturally explains why the mass-loss rates inferred for the progenitors of SNe Ibc span a much larger range than the observed wind mass-loss rates of WRs in our Galaxy (e.g. Soderberg 2007, Wellons et al. 2012). Finally, the indication of non-metallicity driven mass-loss mechanisms being at play in the evolutionary path that leads to Ib/c SNe is also consistent with inferences from the demographics of SN types combined with initial-mass function considerations (Smith et al. 2011).

To explain the observations of SN 2014C we are forced to leave behind the traditional view of single massive star evolution and explore the possibility of alternative physical mechanisms responsible for the ejection of the H envelope of its progenitor, with the following key requirements:

(1) Synchronized with the explosion.

(2) Efficient, and able to (almost) entirely strip the star of its last H layer.

(3) Common to 10% of progenitors of H-stripped SNe during their last ~ 500 years of evolution, but potentially to every SN Ib/c progenitor *if* the process is intrinsically active over a longer time scale of 5000 yrs or more.

We consider below the effects of binary evolution and late-stage nuclear burning instabilities, which are typically not incorporated in the current prescriptions of mass loss in evolved massive stars.

6.2.1. *Binary Interaction*

The ejection of the H-rich envelope can be the result of binary interaction (e.g. Podsiadlowski et al. 1992). Since the majority of young massive stars are found in binary systems that are close enough to interact (e.g. Sana et al. 2012), these ejections are expected to be common, but not necessarily synchronized with the stellar death.

The binary interaction can strip the star of almost all of its H, leaving behind just a thin H layer on its surface (which would be later lost through metallicity-dependent, line-driven winds). The envelope material is expected to get compressed into a thin and dense shell, consistent with what we observe for SN 2014C. Furthermore, a binary progenitor for SN 2014C is also suggested by the pre-explosion observations of the cluster of stars that hosts SN 2014C, which favor lower mass star progenitors with $M < 20\,M_\odot$ (M15). Stars with relatively lower masses are disfavored as progenitors of Ib/c SNe in a single-star progenitor scenario because of their weaker winds, which are not able to entirely strip the star of its H-envelope. Stars with relatively lower masses are instead the most common progenitors of Ib/c SNe in a binary progenitor scenario, where the interaction with the companion would bear the burden of the envelope removal. Finally, since the observed fraction of $\sim 37\%$ of H-poor SNe among core-collapse explosions is too large to be reconciled with the evolution of

single massive stars (e.g. Kobulnicky & Fryer 2007, Eldridge et al. 2008, Li et al. 2011, Smith et al. 2011), it is expected that at least a fraction of SNe Ibc originate in binaries.

However, in general we do not expect the stellar death and the binary interaction to be related events that are synchronized in time. The time lag between the interaction and stellar death can be small if the progenitor fills its Roche lobe in a late evolutionary stage. This occurs for systems with orbital periods longer than ~ 1000 days that undergo case-C mass transfer (e. g. Fig. 1 in Schneider et al. 2015). In such systems the progenitor fills its Roche lobe as a red super giant, after finishing central helium burning. At this stage the star typically has less than a few thousand years (depending on its mass) to live until its final explosion. The convective envelope of the giant responds to mass loss by expanding, leading to dynamically unstable mass transfer in which the companion is engulfed in the envelope of the red supergiant. The envelope is ejected as the companion spirals in, which takes a few orbits at most (Ivanova et al. 2013). This means that several solar masses of hydrogen rich material are ejected within a short time ($\lesssim 1$ year), leading to a dense shell, torus or disk around the binary system.

The outflow velocities of the H-rich material are expected to be comparable to the escape speed of the surface of the original red supergiant (up to a few $10\,\mathrm{km\,s^{-1}}$), or possibly even less if the material remains bound to the system and resides in a circum-binary disk. It is unclear how long the ejected material can survive in the vicinity of the system. The ejected material will be shaped and eventually eroded by the fast line-driven wind of the stripped progenitor and its ionizing photons (Metzger 2010).

Case-C mass transfer is relatively rare for binary systems where the primary is massive enough to produce a SN. Podsiadlowski et al. (1992) estimate this fraction to be 5.6% among binary systems with primaries with mass in the range $8-20\,M_\odot$. For a more accurate estimate of this fraction and to obtain the distribution of time lags we use the binary star population synthesis code binary_c (Izzard et al. 2009, 2006, 2004; de Mink et al. 2013) which relies on the algorithms by Hurley et al. (2000, 2002). The crucial ingredients in this estimate are the stellar lifetimes and radial expansion of the stars, which follow from the detailed stellar evolutionary models by Pols et al. (1998). These algorithms provide a computationally efficient approximation that allows to simulate a full population of binary systems. The approximations are sufficient for the scope of this work, but future investigation with detailed codes would be desirable.

We simulate binary populations by choosing primary masses from a Kroupa (2001) mass function and companion masses uniformly distributed with a mass ratio between 0.1 and 1 (e.g. Duchêne & Kraus 2013; Sana et al. 2012). We assume a uniform distribution of initial periods p in log space (Öpik's law). However, for systems with initial masses above $15\,M_\odot$ we adopt the distribution obtained by Sana et al. (2012) that more strongly favors short period systems, with $0.15 \leq \log_{10} p \leq 3.5$. We assume a binary fraction of 0.7. We account for the relevant physical processes that govern binary systems including stellar wind mass loss, Roche-lobe overflow and common envelope (CE) phases using the standard assumptions for the physics parameters as summarized in de Mink et al. (2013) and references therein. In addition, apart from our standard model we also run simulations with different assumptions for the initial conditions (i.e. slope of

the initial mass function, binary fraction, distribution of mass ratios and orbital periods) and the treatment of the physical processes (i. e. efficiency of common envelope ejection, efficiency of mass transfer, critical mass ratio for the onset of contact, amount of mixing and mass loss assumed during a stellar merger). We find that the variations in the initial mass function dominate the uncertainty. We refer to de Mink et al. (2013), de Mink et al. (2014) and Izzard et al. (2004) for a detailed discussion. The full set of simulations will be published in Zapartas et al. (in prep).

We find that $\sim 6.5\%$ (3.8 − 10%) of type Ibc SN progenitors result from systems that experienced case-C CE evolution. The 3.8 − 10% range reflects a variation of the slope of the initial mass function $\alpha_{IMF} = -2.3 \pm 0.7$. The other parameters of our model induce smaller variations to the final fraction of progenitors that went through case-C CE evolution. The fraction of progenitors with recent CE evolution is thus somewhat smaller than -but reasonably close to- our estimates of interacting systems of Sec. 5. The typical progenitors are stars of $8 - 20 M_\odot$ in wide binary systems of $\gtrsim 1000$ days, which experience unstable mass transfer and CE after their core He exhaustion. At this stage, the life time before core collapse is similar to the time scale for carbon burning, which is typically a few 10^3 yrs, but potentially extends to a few 10^4 yrs for the lowest-mass progenitors (Jones et al. 2013). This fact implies that binary interaction can be the main culprit *if* the material ejected during the CE phase is able to survive close to the system for a few $\sim 10^3 - 10^4$ yrs.

Alternatively we need to invoke a new physical mechanism or more exotic channels to enhance the fraction of Ibc SNe with CE interaction shortly before the explosion. A possibility is to consider exotic binary evolutionary channels where the final explosion has a causal relation with the binary interaction. One example is the reverse CE inspiral of a neutron star or black hole in the envelope of the companion as discussed by Chevalier (2012). Based on the estimates by Chevalier (2012) this channel would be able to account for 1-3% Ibc SNe. Alternatively, the fraction of interacting systems can be increased if the stellar radius of the progenitor inflates before the explosion. Instabilities during the last phases of nuclear burning evolution might inject the necessary energy that leads to the envelope inflation (Smith & Arnett 2014), and might explain the larger fraction of interacting Ibc supernovae in our sample.

6.2.2. *Instabilities during the final Nuclear Burning Stages*

Instabilities associated with the final nuclear burning sequences (especially O and Ne) have been recently invoked to explain the observation of eruptions from massive stars in the months to years before core collapse (Arnett & Meakin 2011b, Quataert & Shiode 2012, Shiode et al. 2013, Shiode 2013, Smith & Arnett 2014). This mechanism is naturally synchronized with the stellar demise and it is expected to be common to most stars. However, nuclear burning instabilities do not necessarily lead to the almost complete stripping of the H layer that we observe in SN 2014C. Even more importantly, our observations of SN 2014C require the H envelope ejection to have happened ≥ 20 years before the explosion, definitely *before* the start of the O-burning phase. Heavy mass loss in the H-stripped SN 2014C was thus not limited to the few years preceding the collapse, and, if connected to nuclear burning instabilities, directly points to the development of instabilities even at earlier times in the nuclear burning sequence.

Current theoretical investigations have explored with realistic simulations only the very late nuclear burning stages (O, Ne and later stages, with duration of the order of $\sim$ yrs) mainly because of limitations in computational power (Meakin 2006, Arnett & Meakin 2011a, Smith & Arnett 2014, Smith 2014). SN 2014C and our analysis of type Ib/c SNe of Sec. 5.2 is however suggestive of a significantly longer active time of the physical process behind the ejection of massive H-rich material. For $v_H \leq 1000 \, \mathrm{km \, s^{-1}}$, $\Delta t_{active} \geq 5000$ yrs, thus extending well back into the C-burning stage of massive stars (e.g. Yoon & Cantiello 2010; Shiode & Quataert 2014).

It is thus urgent to theoretically explore the possibility of instabilities during the earlier stages of nuclear burning, potentially extending to C-burning.[20] The -so far- neglected time dependence of nuclear burning and mass loss in massive stars might have a fundamental influence on the pre-SN structure of the progenitor star, a key input parameter to all numerical simulations of SN explosions (Janka 2012).

7. SUMMARY AND CONCLUSIONS

SN 2014C represents the first case of a SN originating from an H-stripped progenitor for which we have been able to closely monitor a complete metamorphosis from an ordinary Ib-SN into a strongly interacting type-IIn SN over a time scale of ~ 1 yr (Milisavljevic et al. 2015). Observational signatures of this evolution appear across the electromagnetic spectrum, from the hard X-rays to the radio band. The major finding from our study of SN 2014C is the presence of substantial ($M \sim 1 M_\odot$) H-rich material located at $R \sim 6 \times 10^{16}$ cm from the explosion site of an H-poor core-collapse SN. This phenomenon challenges the current theories of massive stellar evolution and argues for a revision of our understanding of mass loss in evolved massive stars. Specifically:

- With $E_k \sim 1.8 \times 10^{51}$ erg, $M_{ej} \sim 1.7 M_\odot$ and $M_{Ni} \sim 0.15 M_\odot$, the explosion parameters of SN 2014C are unexceptional among the population of Ib/c SNe.

- SN 2014C adds to the complex picture of mass loss in massive stars that recent observations are painting (Smith 2014) and demonstrates that the ejection of massive H-rich material is not a prerogative of very massive H-rich stars ($M \sim 60 M_\odot$, like the progenitor of SN 2009ip, Smith et al. 2010, Foley et al. 2011). Instead it shows that even progenitors of normal H-poor SNe can experience severe pre-SN mass loss as late as $10 \lesssim t \lesssim 1000$ years before explosion. Heavy mass loss in SNe Ib/c is thus not limited to the few years preceding core collapse.

- In this sense SN 2014C bridges the gap between ordinary SNe Ib/c and type-IIn SNe, which show signs of shock interaction with a dense medium from the very beginning. The existence of 14C-like events establishes a continuum of time-scales of ejection of substantial H-rich material by massive stars, extending from < 1 yr

---

[20] While the exact time scales of each burning stage is sensitive to the currently imposed mass-loss rates in stellar evolution models which do not include the effects of time-dependent mass loss discussed in this section, we note that the detection of infrared echoes from distant shells in the environments of IIn (e.g. Fox et al. 2011) and non-IIn SNe (an illustrative example is the ring of material at $\sim 6 \times 10^{17}$ cm from the explosion site of SN 1987A, Sonneborn et al. 1998) independently supports the idea that enhanced mass loss is not confined to the few years before the stellar collapse.

TABLE 3
Swift-UVOT PHOTOMETRY.

Date (d)	v (mag)	Date (d)	b (mag)	Date (d)	u (mag)	Date (d)	w1 (mag)	Date (d)	w2 (mag)	Date (d)	m2 (mag)
663.25[a]	15.29(0.06)[b]	663.25	16.35(0.06)	663.25	16.46(0.08)	663.28	17.84(0.13)	663.25	>18.68	663.26	>18.93
664.18	15.18(0.07)	664.21	16.17(0.06)	664.21	16.54(0.08)	664.21	17.69(0.10)	664.21	>18.93	664.22	>19.12
664.25	15.15(0.06)	666.45	15.85(0.05)	666.45	16.34(0.07)	666.59	17.73(0.07)	960.21	>19.10	960.21	>19.03
666.45	14.79(0.04)	666.52	15.81(0.05)	668.45	16.46(0.07)	668.59	17.76(0.07)	1013.69	>19.15		
666.52	14.80(0.04)	668.52	15.81(0.05)	668.52	16.41(0.07)	670.39	17.80(0.07)				
668.52	14.68(0.06)	670.45	15.81(0.05)	670.45	16.66(0.08)	672.46	17.88(0.07)				
670.45	14.69(0.04)	670.52	15.83(0.05)	672.52	16.63(0.08)	674.73	18.00(0.08)				
670.52	14.67(0.04)	672.39	15.91(0.05)	674.79	16.75(0.08)	676.32	17.94(0.07)				
672.39	14.71(0.04)	672.52	15.87(0.05)	676.06	16.83(0.08)	960.21	>18.27				
672.52	14.69(0.04)	674.12	15.96(0.05)	676.59	16.76(0.08)						
674.12	14.77(0.04)	674.80	16.02(0.05)	1044.80	>17.25						
674.80	14.78(0.04)	676.06	16.11(0.05)								
676.06	14.83(0.04)	676.59	16.04(0.05)								
676.59	14.80(0.04)										

[a]Dates are in MJD-56000 (days).
[b]Not host subtracted. Not extinction corrected. Uncertainties are 1σ.

before collapse for type-IIn SNe, to decades and centuries before explosion for Ib/c SNe. This fact leads to the idea that a fraction of spectroscopically classified type-IIn SNe in fact harbor bare Ib/c-like cores that underwent a very recent ejection of their H-rich envelopes.

- SN 2014C violates the expectations from the standard metallicity-dependent line-driven mass loss channel and demonstrates the existence of a time-dependent mass loss mechanism that is active during the last centuries of evolution of some massive stars and that leads to progenitors of ordinary H-poor core-collapse SNe. Possibilities include the effects of the interaction with a binary companion or instabilities during the last nuclear burning stages. In both cases we do not expect a strong metallicity dependence.

- We analyzed 183 Ib/c SNe with radio observations and we found that 10% of SNe in our sample displays evidence for late-time interaction reminiscent of SN 2014C. This fraction is somewhat larger than -but in reasonable agreement with- the expected outcome from recent envelope ejection due to binary evolution *assuming* that the envelope material can survive close to the progenitor site for $10^3 - 10^4$ yrs. Alternatively, events related to the last phases of nuclear burning might also play a critical role providing the energy and the trigger mechanism that cause the ejection of envelope material from an evolved massive star.

- In particular, our analysis suggests that unsteady nuclear burning (i) may be spread across a wide range of initial progenitor mass to include not only the most massive stars, but also ordinary progenitors of Ib/c SNe; (ii) instabilities are not confined to the O, Ne and Si-burning phases, but instead likely extend all the way to C-burning; (iii) unsteady nuclear burning might enhance the fraction of binary interactions before collapse.

The findings and conclusions above highlight the important role of time-dependent, eruptive mass loss in the evolutionary path that leads to the progenitors of ordinary H-poor core-collapse SNe. *The incorrect use of time averaged mass-loss prescriptions in current models of stellar evolution might have a major effect on our understanding of the stellar structure of a massive stellar progenitor approaching core collapse and might lead to inaccuracies in pre-SN stellar structure that are of fundamental importance at the time of the explosion.* To make progress it is urgent to theoretically explore the presence of instabilities during the earlier stages of nuclear evolution in massive stars, and in general, to study the effects of significant eruptive mass loss on the pre-supernova stellar structure. Observationally, it is mandatory to consistently sample the pre-SN life of stellar progenitors in the *centuries* before explosion, a territory that can only be probed with late-time radio and X-ray observations of nearby stellar explosions.

TABLE 4
MMTCam photometry.

Date	r	i
795 [a]	17.34(0.01)[b]	17.05(0.02)
977	18.86(0.05)	18.89(0.08)
1132	19.64(0.09)	19.57(0.13)
1162	19.60(0.09)	19.65(0.14)
1165	19.50(0.11)	19.53(0.14)

[a]Dates are in MJD-56000 (days).
[b]Not host subtracted. Not extinction corrected. Uncertainties are 1σ.

TABLE 5
Sample of 183 Ib/c SNe with radio observations

1954A	1983N	1984L	1985F	1990B	1990U	1991A	1991N	1991ar
1994I	1994ai	1996D	1996aq	1997B	1997C	1997X	1997dc	1998bw
1998T	1999bc	1999di	1999dn	1999ec	1999eh	1999ex	2000C	2005C
2000F	2000H	2000S	2000ds	2000dv	2000cr	2000ew	2000fn	2001B
2001M	2001ai	2001bb	2001ch	2001ci	2001ef	2001ej	2001em	2001is
2002J	2002ap	2002bl	2002bm	2002cj	2002cp	2002dg	2002dn	2002ge
2002gy	2002hf	2002hn	2002ho	2002hy	2002hz	2002ji	2002jj	2002jp
2002jz	2003I	2003L	2003ih	2003kb	2003jg	2003jd	2003is	2003ig
2003hp	2003id	2003gk	2003gf	2003ev	2003el	2003ds	2003dr	2003dg
2003cr	2003bu	2003bp	2003bm	2003aa	2003I	2003H	2003A	2004ao
2004ax	2004aw	2004bf	2004bi	2004bm	2004bs	2004bw	2004bu	2004cc
2004dc	2004dk	2004dn	2004dx	2004eh	2004eu	2004fe	2004ff	2004ge
2004gk	2004gq	2004gt	2004gv	2005E	2005C	2005V	2005N	2005O
2005aj	2005ar	2005az	2005bf	2005bh	2005bj	2005bk	2005bq	2005ce
2005ct	2005da	2005cz	2005dg	2005ek	2005eo	2005hg	2005ke	2005kl
2005kf	2005kz	2005la	2005lr	2005mf	2005nb	2006F	2006ab	2006bf
2006bk	2006cb	2006ck	2006dj	2006dl	2006dg	2006dn	2006ea	2006eg
2006ei	2006ec	2006ep	2006el	2006fo	2006gi	2006jc	2006lt	2007C
2007D	2007I	2007Y	2007bg	2007cl	2007gr	2007iq	2007ke	2007ru
2007rz	2007uy	2008D	2008du	2008dv	2009bb	2010ay	PTF11qcj	2012ap
2012au	2013ge	2014ad						

APPENDIX

TABLES

REFERENCES

08. 1

Anderson, J. P., James, P. A., Habergham, S. M., Galbany, L., & Kuncarayakti, H. 2015, PASA, 32, 19

Arnett, W. D. 1982, ApJ, 253, 785

Arnett, W. D., & Meakin, C. 2011a, ApJ, 733, 78

Arnett, W. D., & Meakin, C. 2011b, ApJ, 741, 33

Bastian, N., Covey, K. R., & Meyer, M. R. 2010, ARA&A, 48, 339

Berger, E., Kulkarni, S. R., Frail, D. A., & Soderberg, A. M. 2003, ApJ, 599, 408

Bietenholz, M. F., & Bartel, N. 2005, ApJ, 625, L99

Bietenholz, M. F., Bartel, N., & Rupen, M. P. 2002, ApJ, 581, 1132

Bietenholz, M. F., De Colle, F., Granot, J., Bartel, N., & Soderberg, A. M. 2014, MNRAS, 440, 821

Björnsson, C.-I., & Fransson, C. 2004, ApJ, 605, 823

Brown, P. J., et al. 2009, AJ, 137, 4517

Burrows, D. N., et al. 2005, Space Sci. Rev., 120, 165

Cano, Z. 2013, MNRAS, 434, 1098

Cano, Z., & Jakobsson, P. 2014, ArXiv e-prints

Cano, Z., Maeda, K., & Schulze, S. 2014, MNRAS, 438, 2924

Chandra, P., Chevalier, R. A., Chugai, N., Fransson, C., Irwin, C. M., Soderberg, A. M., Chakraborti, S., & Immler, S. 2012, ApJ, 755, 110

Chevalier, R. A. 1982, ApJ, 258, 790

Chevalier, R. A. 1984, ApJ, 280, 797

Chevalier, R. A. 2012, ApJ, 752, L2

Chevalier, R. A., & Fransson, C. 2003, in Lecture Notes in Physics, Berlin Springer Verlag, Vol. 598, Supernovae and Gamma-Ray Bursters, ed. K. Weiler, 171

Chevalier, R. A., & Fransson, C. 2006, ApJ, 651, 381

Chevalier, R. A., & Liang, E. P. 1989, ApJ, 344, 332

Chugai, N. N., & Chevalier, R. A. 2006, ApJ, 641, 1051

Clocchiatti, A., & Wheeler, J. C. 1997, ApJ, 491, 375

Corsi, A., et al. 2014, ApJ, 782, 42

Crowther, P. A. 2007, ARA&A, 45, 177

de Jager, C., Nieuwenhuijzen, H., & van der Hucht, K. A. 1988, A&AS, 72, 259

de Mink, S. E., Langer, N., Izzard, R. G., Sana, H., & de Koter, A. 2013, ApJ, 764, 166

de Mink, S. E., Sana, H., Langer, N., Izzard, R. G., & Schneider, F. R. N. 2014, ApJ, 782, 7

Dewey, D., Bauer, F. E., & Dwarkadas, V. V. 2011, in American Institute of Physics Conference Series, Vol. 1358, American Institute of Physics Conference Series, ed. J. E. McEnery, J. L. Racusin, & N. Gehrels, 289

Drout, M. R., et al. 2015, ArXiv e-prints

Drout, M. R., et al. 2011, ApJ, 741, 97

Duchêne, G., & Kraus, A. 2013, ARA&A, 51, 269

Dwarkadas, V. V. 2005, ApJ, 630, 892

Dwarkadas, V. V. 2007, Ap&SS, 307, 153

Dwarkadas, V. V., Dewey, D., & Bauer, F. 2010, MNRAS, 407, 812

Eldridge, J. J., Izzard, R. G., & Tout, C. A. 2008, MNRAS, 384, 1109

Filippenko, A. V., & Chornock, R. 2001, IAU Circ., 7737, 3

Foley, R. J., Berger, E., Fox, O., Levesque, E. M., Challis, P. J., Ivans, I. I., Rhoads, J. E., & Soderberg, A. M. 2011, ApJ, 732, 32
Foley, R. J., Smith, N., Ganeshalingam, M., Li, W., Chornock, R., & Filippenko, A. V. 2007, ApJ, 657, L105
Fox, O. D., et al. 2011, ApJ, 741, 7
Fransson, C., Lundqvist, P., & Chevalier, R. A. 1996, ApJ, 461, 993
Fraser, M., et al. 2013, ApJ, 779, L8
Freedman, W. L., et al. 2001, ApJ, 553, 47
Gehrels, N., et al. 2004, ApJ, 611, 1005
Heger, A., Fryer, C. L., Woosley, S. E., Langer, N., & Hartmann, D. H. 2003, ApJ, 591, 288
Hopkins, A. M., & Beacom, J. F. 2006, ApJ, 651, 142
Humphreys, R. M., & Davidson, K. 1994, PASP, 106, 1025
Hurley, J. R., Pols, O. R., & Tout, C. A. 2000, MNRAS, 315, 543
Hurley, J. R., Tout, C. A., & Pols, O. R. 2002, MNRAS, 329, 897
Ivanova, N., et al. 2013, A&A Rev., 21, 59
Izzard, R. G., Dray, L. M., Karakas, A. I., Lugaro, M., & Tout, C. A. 2006, A&A, 460, 565
Izzard, R. G., Glebbeek, E., Stancliffe, R. J., & Pols, O. R. 2009, A&A, 508, 1359
Izzard, R. G., Tout, C. A., Karakas, A. I., & Pols, O. R. 2004, MNRAS, 350, 407
Janka, H.-T. 2012, Annual Review of Nuclear and Particle Science, 62, 407
Jones, S., et al. 2013, ApJ, 772, 150
Kalberla, P. M. W., Burton, W. B., Hartmann, D., Arnal, E. M., Bajaja, E., Morras, R., & Pöppel, W. G. L. 2005, A&A, 440, 775
Kamble, A., et al. 2015, ArXiv e-prints
Kamble, A., et al. 2014, ApJ, 797, 2
Kelly, P. L., & Kirshner, R. P. 2012, ApJ, 759, 107
Kiewe, M., et al. 2012, ApJ, 744, 10
Kim, M., et al. 2014, Central Bureau Electronic Telegrams, 3777, 1
Kobulnicky, H. A., & Fryer, C. L. 2007, ApJ, 670, 747
Kroupa, P. 2001, MNRAS, 322, 231
Li, W., et al. 2011, Nature, 480, 348
Liedahl, D. A., Osterheld, A. L., & Goldstein, W. H. 1995, ApJ, 438, L115
Lyman, J., Bersier, D., James, P., Mazzali, P., Eldridge, J., Fraser, M., & Pian, E. 2014, ArXiv e-prints
Madau, P., Pozzetti, L., & Dickinson, M. 1998, ApJ, 498, 106
Maeda, K., et al. 2015, ApJ, 807, 35
Margutti, R., et al. 2015, ApJ, 805, 159
Margutti, R., et al. 2014a, ApJ, 780, 21
Margutti, R., et al. 2014b, ApJ, 797, 107
Margutti, R., et al. 2012, ApJ, 751, 134
Marshall, J. R., van Loon, J. T., Matsuura, M., Wood, P. R., Zijlstra, A. A., & Whitelock, P. A. 2004, MNRAS, 355, 1348
Massey, P., Neugent, K. F., & Morrell, N. 2015, ApJ, 807, 81
Matzner, C. D., & McKee, C. F. 1999, ApJ, 510, 379
Mauerhan, J. C., et al. 2013, MNRAS, 430, 1801
Mauron, N., & Josselin, E. 2011, A&A, 526, A156
Meakin, C. A. 2006, Ph.D. thesis, The University of Arizona, Arizona, USA
Metzger, B. D. 2010, MNRAS, 409, 284
Mewe, R., Gronenschild, E. H. B. M., & van den Oord, G. H. J. 1985, A&AS, 62, 197
Mewe, R., Lemen, J. R., & van den Oord, G. H. J. 1986, A&AS, 65, 511
Milisavljevic, D., Fesen, R. A., Leibundgut, B., & Kirshner, R. P. 2008, ApJ, 684, 1170
Milisavljevic, D., et al. 2015, ApJ, 815, 120

Moffat, A. F. J. 2008, in Clumping in Hot-Star Winds, ed. W.-R. Hamann, A. Feldmeier, & L. M. Oskinova, 17
Nakar, E. 2015, ApJ, 807, 172
Ofek, E. O., et al. 2013, Nature, 494, 65
Ofek, E. O., et al. 2014, ApJ, 789, 104
Pastorello, A., et al. 2015, MNRAS, 449, 1921
Pastorello, A., et al. 2013, ApJ, 767, 1
Pastorello, A., et al. 2007, Nature, 447, 829
Piro, A. L., & Nakar, E. 2013, ApJ, 769, 67
Piro, A. L., & Nakar, E. 2014, ApJ, 784, 85
Podsiadlowski, P., Joss, P. C., & Hsu, J. J. L. 1992, ApJ, 391, 246
Pols, O. R., Schröder, K.-P., Hurley, J. R., Tout, C. A., & Eggleton, P. P. 1998, MNRAS, 298, 525
Quataert, E., & Shiode, J. 2012, MNRAS, 423, L92
Ramirez-Ruiz, E., Dray, L. M., Madau, P., & Tout, C. A. 2001, MNRAS, 327, 829
Romano, P., Guidorzi, C., Segreto, A., Ducci, L., & Vercellone, S. 2014, A&A, 572, A97
Roming, P. W. A., et al. 2005, Space Sci. Rev., 120, 95
Rupen, M. P., van Gorkom, J. H., Knapp, G. R., Gunn, J. E., & Schneider, D. P. 1987, AJ, 94, 61
Salas, P., Bauer, F. E., Stockdale, C., & Prieto, J. L. 2013, MNRAS, 428, 1207
Sana, H., et al. 2012, Science, 337, 444
Schinzel, F. K., Taylor, G. B., Stockdale, C. J., Granot, J., & Ramirez-Ruiz, E. 2009, ApJ, 691, 1380
Schlafly, E. F., & Finkbeiner, D. P. 2011, ApJ, 737, 103
Schneider, F. R. N., Izzard, R. G., Langer, N., & de Mink, S. E. 2015, ApJ, 805, 20
Shiode, J. H. 2013, Ph.D. thesis, University of California, Berkeley
Shiode, J. H., & Quataert, E. 2014, ApJ, 780, 96
Shiode, J. H., Quataert, E., Cantiello, M., & Bildsten, L. 2013, MNRAS, 430, 1736
Smith, N. 2014, ARA&A, 52, 487
Smith, N., & Arnett, W. D. 2014, ApJ, 785, 82
Smith, N., Li, W., Filippenko, A. V., & Chornock, R. 2011, MNRAS, 412, 1522
Smith, N., Mauerhan, J. C., Silverman, J. M., Ganeshalingam, M., Filippenko, A. V., Cenko, S. B., Clubb, K. I., & Kandrashoff, M. T. 2012, MNRAS, 426, 1905
Smith, N., et al. 2010, AJ, 139, 1451
Smith, N., & Owocki, S. P. 2006, ApJ, 645, L45
Soderberg, A. 2007, Ph.D. thesis, California Institute of Technology
Soderberg, A. M., et al. 2010, Nature, 463, 513
Soderberg, A. M., Nakar, E., Berger, E., & Kulkarni, S. R. 2006, ApJ, 638, 930
Sonneborn, G., et al. 1998, ApJ, 492, L139
Spitzer, L. 1962, Physics of Fully Ionized Gases
Svirski, G., & Nakar, E. 2014, ApJ, 788, L14
Tinyanont, S., et al. 2016, ArXiv e-prints
Valenti, S., et al. 2008, MNRAS, 383, 1485
van Loon, J. T., Cioni, M.-R. L., Zijlstra, A. A., & Loup, C. 2005, A&A, 438, 273
Wellons, S., Soderberg, A. M., & Chevalier, R. A. 2012, ApJ, 752, 17
Wheeler, J. C., Johnson, V., & Clocchiatti, A. 2015, MNRAS, 450, 1295
Yan, L., et al. 2015, ArXiv e-prints
Yoon, S.-C., & Cantiello, M. 2010, ApJL, 717, L62